Title

Mechanisms of Nicotinic Acetylcholine Receptor Regulation By NACHO and Members of the Ly6 Family

Author

Liu, Clifford Zhuo

Publication Date

2017

Peer reviewed|Thesis/dissertation

UNIVERSITY OF CALIFORNIA, SAN DIEGO

Mechanisms of Nicotinic Acetylcholine Receptor Regulation By NACHO and Members of the Ly6 Family

A Thesis submitted in partial satisfaction of the requirements
for the degree Master of Science

in

Biology

by

Clifford Zhuo Liu

Committee in charge:

Professor William Joiner, Chair
Professor Darwin Berg, Co-Chair
Professor Jing Wang

2017

The Thesis of Clifford Zhuo Liu is approved and it is acceptable in quality and form for publication on microfilm and electronically:

Co-Chair

Chair

University of California, San Diego

2017

TABLE OF CONTENTS

LIST OF ABBREVIATIONS

ACh: acetylcholine

Aβ: beta-amyloid protein

CaMKII: Ca^{2+}- calmodulin dependent kinase II

CREB: cAMP response element-binding protein

ER: endoplasmic reticulum

GABA: γ-aminobutyric acid type A

GPI: glycosylphosphatidylinositol

MAPK: mitogen activated protein kinase

nAChRs: nicotinic acetylcholine receptors

PI3K: phosphatidylinositol 3-kinase

PKA: protein kinase A

PNGase-F: Peptide-N-glycosidase F

Ric3: Resistant to Inhibitors of Cholinesterase

SSS: sleepless

VTA: ventral tegmental area

5-HT_3: 5-hydroxytryptamine type 3

LIST OF FIGURES

Chapter 1

Chapter 2

ACKNOWLEDGEMENTS

I would first like to thank Professor William Joiner for his support throughout the years I have been in his lab. His guidance throughout my time in his lab has been invaluable in not only the completion of this thesis, but also in shaping my career path and the type of scholar I aspire to become.

I would also like to acknowledge Dr. Meilin Wu, who has taught me most of my lab skills and has helped me troubleshoot countless experiments. Without her guidance, my progress would have been significantly slower. Furthermore, I would also like to thank her for countless discussions on my career path—the impact of which is immeasurable.

Additionally, I would like to thank all current and previous members of the Joiner Lab, who have kept me company during long nights and supported me during my most stressful times.

Lastly, I would like to acknowledge my committee, who have been supportive of my work presented in this thesis.

Chapter 1, in part is in the final stages before submission for publication. I was the primary investigator and author of this material. Dr. Meilin Wu and Erika Barrall (undergraduate student) were also invaluable in obtaining these results.

Chapter 2, in part, is a reprint of the material as it appears in PlosONE 2016. Wu, Meilin; Liu, Clifford Z.; Joiner, William J., PlosONE, 2016. I was the second author of this paper.

ABSTRACT OF THE THESIS

Mechanisms of Nicotinic Acetylcholine Receptor Regulation
By NACHO and members of the Ly6 family

by

Clifford Zhuo Liu

Master of Science in Biology

University of California, San Diego, 2017

Professor William Joiner, Chair
Professor Darwin Berg, Co-Chair

Dysregulation of nicotinic acetylcholine receptors (nAChRs) is implicated in a wide variety of disorders, including nicotine addiction and Alzheimer's disease. However, it has been challenging to target nAChRs pharmacologically in disease states because the receptors are comprised of structurally similar subunits that are found

broadly throughout the nervous system. Another challenge is avoiding excessive activation of these receptors, which can cause cytotoxicity. One way to circumvent these challenges could be to identify and target different proteins that regulate and modulate nAChRs. In this thesis, we describe two such proteins, Ly6h in mammals and Sleepless in flies; we describe the mechanisms by which these Ly6 proteins regulate nAChRs; and we identify structural motifs that enable these regulatory functions. Specifically, using ion flux assays, co-immunoprecipitations, surface labeling, and confocal microscopy, we show that both Ly6h and Sleepless utilize a single loop to interact with and inhibit nAChRs, at least in part by preventing accumulation of functional receptors on the cell surface. Additionally, in mammalian cells we identify direct antagonism between Ly6h and NACHO, a recently discovered chaperone that can accelerate the assembly of nAChRs. We demonstrate that this antagonism between Ly6h and NACHO is likely to result from competition for binding and assembly of nAChRs. These studies provide insight into mechanisms through which nAChRs are likely to be tightly regulated, which may help in the design of novel drugs to modulate cholinergic signaling in disease states.

Introduction

Nicotinic acetylcholine receptors (nAChRs) are ligand-gated ion channels found in neurons and muscle that are activated by the endogenous neurotransmitter acetylcholine (ACh). nAChRs belong to the Cys-loop receptor superfamily, which also includes 5-hydroxytryptamine type 3 (5-HT_3) receptors, γ-aminobutyric acid type A ($GABA_A$) receptors, and glycine receptors (*1*). Neuronal nAChRs can form homopentamers consisting of only α7 subunits or heteropentamers consisting of various combinations of α subunits (α2-α10) and β subunits (β2-β4) (*2, 3*). When activated, each of the five transmembrane subunits rearrange to rapidly open a nonselective cation channel, allowing sodium, potassium, and in some cases calcium ions to flow through (*3*). Depending on the subunit composition, nAChRs can desensitize rapidly within milliseconds (α7), or slowly over the course of a few seconds (non- α7 heteropentamers) (*4*). In the peripheral nervous system nAChRs are postsynaptic mediators of sympathetic and parasympathetic ganglionic signaling as well as synaptic transmission at the neuromuscular junction. In the central nervous system nAChRs also mediate postsynaptic signaling to ACh, but in some neurons they additionally regulate presynaptic neurotransmitter release, neuronal excitability, calcium-dependent intracellular signaling, and synaptic plasticity (*5-7*). In these capacities nAChRs contribute to the regulation of sleep/wake cycles, cognition and memory, and critical periods in brain development (*8-12*).

The importance of these nAChRs are highlighted in the pathological consequences resulting from their dysregulation in disease states. One such example is

nicotine addiction. The major nAChR subtype implicated in this condition is the α4β2 receptor, which not only has a high affinity for nicotine, but is also expressed in the mesolimbic reward pathway, which includes the ventral tegmental area (VTA) (*13, 14*). In this brain region α4β2 nAChRs have been shown to be necessary and sufficient for nicotine reinforcement (*15, 16*). At the cellular level nicotine addiction is thought to be caused by nicotine's ability to cross membranes and act as a pharmacological chaperone for nAChRs within the VTA, resulting in changes in receptor stoichiometry and up-regulation of abundance and trafficking of receptors to the plasma membrane (*8, 14, 17*). This pharmacological chaperoning can occur at nanomolar concentrations of nicotine that exist in a person's blood after smoking, and results in a shift in the balance between receptor monomers trapped in the endoplasmic reticulum (ER) to more mature, assembled multimers in the Golgi that are destined for the cell surface to mediate nicotinic signaling (*18, 19*). This process has been most studied in the context of α4β2 nAChRs, in which receptor upregulation in the VTA is thought to contribute to reward during smoking and to craving during abstinence (*14*). Indeed among the only effective smoking cessation drugs is varenicline, a partial agonist of α4β2 nAChRs (*20*). However, α7 nAChRs may also represent unexplored potential pharmacological targets to treat nicotine addiction. Interestingly, activation of α7 receptors has been reported to decrease motivation to self-administer nicotine in mice, whereas antagonism of the receptor leads to an increase in motivation (*20*). In addition, α7 knockout mice also show an increased sensitivity to nicotine (*21*). In this context it is notable that α7 receptors are reduced by ~50% in the frontal cortices of individuals with schizophrenia and that these individuals also have an increased incidence of smoking. An interesting hypothesis is that

schizophrenic patients self-medicate with nicotine in an attempt to compensate for low α7 levels (*22, 23*).

nAChRs have also been hypothesized to play a role in the pathology of Alzheimer's disease. The Beta-amyloid protein (Aβ), which is linked to the pathology of Alzheimer's disease, preferentially accumulates in regions of the brain that contain high levels of nAChRs (*7*). One of these regions is the hippocampus—a region of the brain important for memory and learning. In particular, neurons in the hippocampus express high levels of α7 receptors. The potential involvement of nAChRs in Alzheimer's pathology is underscored by a direct interaction between the pathogenic Aβ and nAChRs and subsequent dysregulation. However, there is a lack of consensus over the consequences of Aβ's interaction with α7 receptors. For example, some studies show that Aβ is able to activate α7 and subsequently activate a mitogen activated protein kinase (MAPK) pathway (*24-26*), while others have shown an inhibitory effect of Aβ on α7 (*27*). There is also disagreement on the mechanism of dysregulation of nAChRs. Some studies have shown that there is a progressive loss of α7 receptors in both Alzheimer's patients and mouse disease models (*28, 29*), whereas other studies have shown an upregulation of α7 and increased neuronal excitability under chronic Aβ conditions (*30*). Although it is unclear how these changes may contribute to disease pathology, one possibility is that dysregulation of α7 nAChRs downregulates endogenous neuroprotective mechanisms. Indeed, multiple studies have shown that activation of nAChRs may prevent glutamatergic excitotoxicity (*8, 11, 31, 32*).

Since the dysregulation of nAChRs has been implicated in various disorders, there is significant interest in identifying compounds that can modulate nicotinic signaling pathways selectively. One approach is to target endogenous modulators of nAChRs, which may show greater structural differences and/or spatial restriction than the different receptor subunits themselves. One challenge to this approach is to identify such endogenous modulators. Another challenge is to understand the mechanisms by which such proteins affect nAChR function. One such protein is Resistant to Inhibitors of Cholinesterase (Ric3), a chaperone that selectively enhances α7-mediated currents (*33, 34*). More recently, several members of the Ly6 family have been shown to alter agonist sensitivity, gating kinetics, subunit stoichiometry or trafficking of different nAChRs (*35-39*). In addition, in 2016, an ER resident protein called NACHO was shown to facilitate assembly of nAChR monomers and thus increase functional pentameric receptor expression on the cell surface (*40, 41*). Other recent efforts to identify additional modulators of nAChRs (*42*) will undoubtedly shed light on the complex regulatory network governing nAChRs. Understanding the endogenous mechanisms of nAChR regulation, especially those that govern the balance between disassembly/assembly and intracellular retention/ surface expression, will provide insight into pharmacological intervention in cholinergic disease states.

Chapter 1: Antagonism between NACHO and Ly6h regulates the function of α7 nAChRs

Recently, a new chaperone of nAChRs was identified as a transmembrane, ER resident protein named NACHO. In particular, NACHO is required to enhance folding, assembly and trafficking of nAChRs throughout the mammalian brain, resulting in a large increase of nAChR-mediated currents in individual neurons (*40*). These chaperone effects appear to be specific to nAChRs alone, without any functional consequences on other ion channels, such as glutamate or serotonin receptors (*40*). However, amongst the different subtypes of nAChRs, NACHO is found to mediate assembly of all nAChRs that have been tested thus far, including abundant subtypes such as α4β2 and α7 receptors (*41*). Interestingly, this upregulation of nAChRs seems to occur by a mechanism that is distinct from the chaperoning effects of nicotine since NACHO and chronic nicotine have additive effects on the surface expression of α4β2 nAChRs (*41*). NACHO may be important particularly during development, since its levels decrease and begin to level off after postnatal day 7 in rats. Furthermore, during chronic nicotine exposure NACHO is only transiently upregulated perinatally, and only in the frontal cortex (*43*). Surprisingly for a protein that is required for nAChR function, NACHO knockout mice are viable, but they show impaired learning and memory (*41*).

Several members of the Ly6 family of proteins have also recently been shown to interact with and modulate nAChR function (*36*). Like snake α-neurotoxins, with which they share significant homology, Ly6 proteins are small, single domain proteins that are predicted to fold into a three-finger motif that is stabilized by 4-5 conserved disulfide

bonds (*44*). Unlike snake α-neurotoxins, which are secreted, most Ly6 proteins appear to be anchored to the plasma membrane by a glycosylphosphatidylinositol (GPI) moiety, although a few Ly6 proteins are also released from cells (*45-47*). Interestingly, Ly6 proteins are not toxic, but are required for normal development and function of the brain. For example, one of the best characterized Ly6 proteins is Lynx1, which was originally discovered to act in the visual cortex of mice to limit adult visual plasticity through inhibition of nAChR activity (*8, 9, 37*). Subsequently, Lynx1 has been shown to regulate α4β2 nAChRs by shifting receptor composition to subunits with low affinity for agonist and by reducing the rate of receptor desensitization (*38, 39*).

Another Ly6 protein that has been recently characterized is Ly6h, which is highly expressed in hippocampal pyramidal neurons. Previous work in our lab has shown that Ly6h is able to stably interact with α7 nAChRs and limit their trafficking to the cell surface. Through knockdown and overexpression experiments our lab demonstrated that this mechanism likely accounts for the necessity and sufficiency of Ly6h for α7-mediated currents in hippocampal pyramidal neurons (*35*). This mechanism may be relevant to both normal and disease physiology since α7 is thought to be important for cognition and for some effects of Aβ in Alzheimer's disease. Given that both NACHO and Ly6h are found in hippocampal neurons, yet appear to have opposing effects, we began to investigate the basis for this antagonism and how it contributes to the regulation of α7 nAChR assembly and function. In addition, we also sought to define the structural contributions of Ly6h that endow this protein with the ability to downregulate α7.

Here, we report that NACHO and Ly6h appear to compete with each other in a common pathway governing nAChR biogenesis. Specifically, we report that whereas NACHO promotes the assembly of mature α7 pentamers, Ly6h inhibits this process. We further show that loop 3 of Ly6h is both necessary and sufficient for this inhibition by interfering with the effects of NACHO. These findings point to a novel mechanism through which endogenous nAChR levels may be tightly regulated. They also point to the novel possibility that imbalance between NACHO and Ly6h could contribute to neuronal pathologies involving cholinergic signaling. Understanding how balance and imbalance is achieved could thus provide novel insights into pharmacological correction in aberrant states.

Results

Antagonism between NACHO and Ly6h on α7

Whole cell recordings have previously shown that NACHO increases α7 mediated currents and acts synergistically with Ric3 (*40*), while Ly6h inhibits α7 currents (*35*). In order to test the differential effects of NACHO and Ly6h on α7 currents we used the ratiometric FRETable calcium reporter TN-XXL to measure nAChR activity as a function of Ca^{2+} influx in transiently transfected HEK-tsa cells (*48*). In our heterologous system, we were therefore able to assay α7 activity in a dose dependent manner with the agonist, nicotine. We found that either Ric3 or NACHO was required for heterologous expression of α7, and that the lack of both resulted in no detectable FRET signal (Fig S1). We also found that NACHO plus Ric3 increased the maximal response of α7 by nearly

50% relative to Ric3 alone, and that the presence of Ric3 in our system did not result in any additional significant effect relative to NACHO alone (Fig 1A-B). Thus, it appears that NACHO is more efficacious than Ric3 in potentiating α7 currents. In contrast, we found that Ly6h alone is able to decrease the maximal response of α7 by roughly 40%. Interestingly, when cells were co-transfected with both NACHO and Ly6h, the maximal response of α7 was shifted back toward values found in control conditions, in the absence of Ly6h and NACHO (Fig 1A-B). These data are consistent with mixed effects of Ly6h and NACHO rather than a dominant effect of either protein.

NACHO and Ly6h also had opposing effects on the EC_{50} of α7 activation. In the presence of NACHO and Ric3 we measured a ~60% reduction in this value relative to Ric3 alone (Fig 1C). Again, the presence of Ric3 did not result in any additional effect relative to NACHO alone. Ly6h, however, was able to significantly increase the EC_{50} by ~60%. An intermediate effect was observed when cells were co-transfected with NACHO and Ly6h together (Fig 1C). In this case, although the EC_{50} was significantly less than in control conditions, it still increased compared to the effect of NACHO in the absence of Ly6h. The decrease in EC_{50} is unexpected, since NACHO is reported to be an ER-resident protein that is not detected at the plasma membrane, and does not form a stable interaction with α7 (*40*). In contrast, because Ly6h interacts with α7 (*35*) and is found at the plasma membrane (Fig 3B), the increase in EC_{50} by Ly6h can be explained by competitive antagonism during receptor activation by nicotine.

Collectively the opposing effects of NACHO and Ly6h support our hypothesis that the two proteins compete for binding to α7, probably in the ER where NACHO has

been reported to be found. Our data suggest that receptors that interact with NACHO in the ER exclude Ly6h, thus leading to enhanced assembly and maximal response as well as minimal competitive antagonism at the cell surface. Our data also suggest that receptors that interact with Ly6h in the ER exclude NACHO, thus leading to reduced assembly and maximal response to agonist, and increased antagonism to agonist by bound Ly6h at the cell surface.

To test our hypothesis that NACHO and Ly6h compete for binding to α7 subunits, we used a YFP-tagged α7 to co-immunoprecipitate Ly6h in the presence or absence of NACHO. We found that in the presence of NACHO, the amount of Ly6h that formed a stable complex with the receptor was significantly decreased by around 70% (Fig 1D-E). We were unable to perform the reciprocal experiment and co-immunoprecipitate NACHO with α7, possibly due to transient and spatially restricted interactions, so we could not test whether Ly6h reduces NACHO binding to nAChRs. Nonetheless, our finding that NACHO can displace Ly6h from binding to α7 subunits supports our hypothesis that NACHO and Ly6h compete for interacting with α7 nAChRs.

De novo structural prediction of Ly6h

Next, we wanted to know the structural basis by which Ly6h contributes to both the inhibition of α7 nAChRs and antagonism of NACHO's effects on these receptors. Since all Ly6 proteins are thought to have a conserved tertiary protein structure consisting of three variable loops stabilized by highly conserved disulfide bonds (*45*), we hypothesized that one or more of these loops would be necessary for the function of

Ly6h. Unfortunately, among Ly6 proteins only the structure of Lynx1 has been solved (*49*). In order to generate an unbiased structural prediction that did not rely on homology to Lynx1, we used the software ROBETTA, which uses lowest free energy analyses, to generate a *de novo* structure of Ly6h. As expected, Ly6h is predicted to fold into a three loop motif, with loop 1 stabilized by a conserved disulfide bond (Fig 2A-B). Although our model did not predict disulfide formation for loops 2 and 3, we suspect that they exist at identified positions in Fig 2B (red spheres) due to their presence at homologous positions in α-neurotoxins with known structures, as well as the presence of conserved cysteines in additional Ly6 proteins (*45*). Similar to other Ly6 proteins which are N-linked glycosylated and glycosylphosphatidylinositol (GPI) linked**,** Ly6h is also predicted to undergo N-linked glycosylation at N56 within loop 1 and to undergo anchorage to members by GPI at N131 (Fig 2A-B).

To determine the functional importance of each loop of Ly6h we proceeded to generate deletion mutants. To avoid destabilizing the structure of Ly6h to such an extent that protein misfolding and degradation resulted, we deleted residues between cysteines predicted to participate in disulfide bond formation. Furthermore, to prevent torsional strain from the loop deletions, a bridge of three alanine residues was used at the loop deletion sites (Fig 2B). These constructs were named Ly6h ΔL1, Ly6h ΔL2, and Ly6h ΔL3. For each of our mutants, we also generated duplicates that contained a C-terminal MYC tag.

Ly6h mutants are stably expressed and undergo normal cellular trafficking to the cell surface

To ensure that our Ly6h mutants were not grossly misfolded and degraded by the cell, we transiently transfected MYC-tagged Ly6h mutants into HEK-tsa cells. Using western blot analysis, we confirmed that all of the Ly6h mutants stably express (Fig 3A). We also confirmed that Ly6h mutants are appropriately post-translationally processed. For example, following treatment with Peptide-N-Glycosidase F (PNGase-F), wildtype Ly6h, ΔL1 and ΔL2 mutants were converted from high into low molecular weight bands of predicted sizes, consistent with predicted N-glycosylation of Ly6h at N131 (Fig 3A). This site falls within loop 1, which is probably why no such size conversion is observed following PNGase-F treatment with the ΔL1 mutant. These experiments show that normal protein processing is not disrupted in any of our deletion mutants. To determine if subcellular trafficking is also preserved in these mutants, we compared the immunostaining pattern of HEK-tsa cells transfected with MYC-tagged wildtype and deletion mutants of Ly6h. We were able to detect surface expression in each case, indicating that removal of any individual loop did not disrupt GPI anchoring to the membrane or appropriate subcellular trafficking signals (Fig 3B). Collectively, these data suggest that all of our Ly6h deletion mutants are stably expressed, appropriately folded, appropriately post-translationally modified, and properly trafficked to the cell surface.

Loop 3 of Ly6h is necessary to stably interact with and inhibit trafficking of α7 to the cell surface

Previous work in our lab and others have shown that numerous members of the Ly6 family of proteins, including Ly6h, are able to form stable complexes with nAChRs and modulate their function (*35, 36, 50*). Using our loop deletion mutants, we asked whether a single loop was required for Ly6h to stably interact with α7 nAChRs. To do so, we transiently transfected our MYC-tagged Ly6h mutant constructs into HEK-tsa cells along with YFP-tagged α7. We then immunoprecipitated the tagged α7 and Western blotted for the presence of the various Ly6h mutants (Fig 4A). We found that all of the Ly6h mutants except for Ly6h ΔL3 were able to co-immunoprecipitate with α7, despite Ly6h ΔL3 being originally present in the cell lysate (Fig 4A). In addition to interactions with α7, we found that loop 3 is also necessary for Ly6h to bind to α4β2 nAChRs, with Ly6h ΔL3 unable to co-immunoprecipitate with GFP-tagged α4 (Fig S2A). In both cases, loss of Ly6h ΔL2 appears to have a weakened interaction with either α7 or α4β2 receptors, as indicated by a weaker immunoprecipitated band (Fig 4A, S2A), perhaps by destabilizing loop 3. These results indicate that loop 3 is necessary for Ly6h to form a stable interaction with both α4β2 and α7 nAChRs.

The mechanism by which Ly6h is thought to inhibit α7 nAChR activity is by regulating trafficking of receptor to the cell surface, resulting in a decrease of overall receptor present at the plasma membrane (*35*). In order to determine the effects of Ly6h on nAChR trafficking, we utilized an extracellular HA-tag on α7. These HA-tagged receptor subunits were then co-transfected into HEK-tsa cells with either MYC-tagged

Ly6h-WT or Ly6h ΔL3. HEK-tsa cells were then incubated with an anti-HA antibody under non-permeabilized conditions prior to lysis, followed by subsequent immunoprecipitation and immunoblot analysis. Using this labeling assay, we found that Ly6h-WT is decreased α7 surface levels by about 50% relative to control. This decrease in surface level of α7 was lost if Ly6h-WT was replaced with Ly6h ΔL3 (Fig 4B). A similar reduction of surface levels can also be seen for α4β2, for which loop 3 of Ly6h is also required (Fig S2B). These results show that loop 3 of Ly6h is necessary to regulate trafficking of both α7 and α4β2 to the plasma membrane, thereby decreasing the amount of receptor present at the cell surface.

Loop 3 of Ly6h is necessary to functionally inhibit α7 nAChRs

In order to assay for the functional consequences of Ly6h-nAChR interactions, we used our flux assay in HEK-tsa cells transfected with α7 and either wildtype Ly6h or Ly6h mutants. By measuring FRET ratios over a range of concentrations of the nAChR agonist nicotine, we generated dose-response curves for the activation of α7. The maximal response in these experiments was significantly reduced by Ly6h-WT to about 50% of control levels (Fig 4C-D). Although all of our Ly6h mutants were able to inhibit the maximal response of α7, the loop 3 mutant had the weakest effect (Fig 4C-D). Ly6h ΔL1 and Ly6h ΔL2 were able to inhibit α7 maximal response by about 35%, while Ly6h ΔL3 was only able to inhibit α7 currents by about 20% (Fig 4D). Therefore, the largest loss of function in relation to Ly6h-WT was the deletion of loop 3, consistent with the inability of Ly6h ΔL3 to form a stable complex and inhibit trafficking of α7 (Fig 4A-B).

Interestingly, loop 3 is also required for inhibition of α4β2 currents (Fig S2C-D). Collectively, these data suggest that loop 3 is necessary for Ly6h to interact with and inhibit both α7 and α4β2 nAChRs by reducing trafficking of receptors to the cell surface.

Loop 3 is sufficient to stably interact with and inhibit α7 *activity*

Next, we asked whether loop 3 alone would be sufficient to mediate a stable interaction with α7 and inhibit its function. To do this, we generated double loop deletion mutants of Ly6h, in which two of the three loops were removed and replaced with three alanines, as described above, resulting in Ly6h mutants with one single loop. We named these mutants Ly6h ΔL2L3, Ly6h ΔL1L3, and Ly6h ΔL1L2.

Using YFP-tagged α7 and MYC-tagged Ly6h double loop deletion mutants, we co-transfected HEK-tsa cells and then immunoprecipitated α7 from total cell lysate. When we immunoblotted for our MYC-tagged proteins, we found that only Ly6h ΔL1L2 and Ly6h-WT were detectable on our blot, despite all of the double mutants being present in the total cell lysate (Fig 5A). The presence of all of our double loop mutants in our input suggests that they were stably expressed and not degraded. Furthermore, our results show that Ly6h ΔL2L3 and Ly6h ΔL1L3 alone are unable to confer a stable interaction with α7, while Ly6h ΔL1L2 is able to. These results suggest that loop 3 alone is sufficient to interact with α7.

To confirm the sufficiency of loop 3 to modulate α7, we then performed our calcium flux assays by co-transfecting HEK-tsa cells with α7 and each of the Ly6h double loop mutants. As expected, α7 alone is activated by its agonist nicotine in a dose-dependent manner, with its maximum response significantly inhibited by Ly6h-WT (Fig

5B-C). Notably the only Ly6h double loop deletion mutant that remains able to inhibit α7 activity is Ly6h ΔL1L2, by ~25% (Fig 5B-C). Although the inhibition by Ly6h ΔL1L2 is not as strong as Ly6h-WT, this is to be expected, since removal of the first two loops may destabilize the conformation of loop 3 and alter the efficacy of Ly6h's interactions with α7. Nonetheless, these data strongly suggest that loop 3 alone is sufficient to both interact with and inhibit α7 activity.

Loop 3 of Ly6h is necessary and sufficient to functionally inhibit and antagonize NACHO mediated assembly of α7 nAChRs

NACHO has been shown to accelerate the assembly of α7 receptors, and our data with Ly6h are consistent with a potential role for it in opposing this process. We hypothesized that loop 3 of Ly6h would be necessary and sufficient to suppress NACHO'S upregulation of α7 by directly antagonizing the assembly of α7 nAChRs. Using our calcium flux assay, we first verified that loop 3 was able to functionally antagonize NACHO's function. Indeed, we found that when loop 3 of Ly6h was deleted, the ability of Ly6h to suppress NACHO'S upregulation of α7 was lost. However, Ly6h's effects were restored with loop 3 alone (Fig 6A-B).

To determine whether Ly6h directly antagonized the assembly of nAChRs by NACHO and whether loop 3 of Ly6h is necessary and sufficient for this antagonism, co-transfected HEK-tsa cells with HA-tagged α7, NACHO and Ly6h mutants. Using biotinylated α-bungarotoxin, which only binds with high affinity to fully formed α7 pentamers (*51-53*), we were able to immunoprecipitate fully formed α7 pentamers from

the total cell lysate. In our preliminary experiments, we found that the presence of NACHO was able to significantly increase the amount of α7 pentamers, with also an increase in the total amount of α7 subunits (Fig 7A-D). Notably, in the absence of NACHO, Ly6h almost completely abolished formation of α7 pentamers. When both NACHO and Ly6h were present together, intermediate levels of assembled receptors were detected (Fig 7A-C). Importantly, loss of loop 3 abolished the ability of Ly6h to inhibit α7 assembly (Fig 7A-B), whereas loop 3 alone seems to inhibit assembly of α7 (Fig 7C). Unfortunately, these preliminary results must be repeated for statistical analyses. Furthermore, in the case of Ly6h ΔL1L2 (Fig 7C-D), the densitometry analysis was confounded by over-saturated pixel density in the NACHO lanes (Fig 7C-D). In future experiments, decreased amount of NACHO cDNA during transfection should help reduce the saturation. Nonetheless, these preliminary data support the hypothesis that loop 3 of Ly6h antagonizes the function of NACHO, resulting in unassembled nAChR subunits trapped in intracellular organelles. In hippocampal neurons, where both proteins have been detected, NACHO and Ly6h are likely to work together to maintain the proper balance of unassembled and assembled α7 subunits so as to maintain cholinergic tone within the appropriate range for normal physiological function.

Discussion

Nicotinic acetylcholine receptors are thought to be potential pharmacological targets for treatment of various disorders of the nervous system, including Alzheimer's disease, schizophrenia, and nicotine addiction. One of the nAChR subtypes, α7, has been

a particularly attractive drug target due to its ability to regulate neurotransmitter release pre-synaptically and to activate signaling cascades post-synaptically to influence cognition (*54, 55*). Additionally, evidence suggests that α7 may have neuroprotective properties, particularly in the hippocampus, which allow neurons to survive from glutamatergic excitotoxicity (*31, 56*). Lastly, α7 activation has been shown to reduce nicotine addiction in mice, whereas the activation of α4β2 contributes to the addictive properties of nicotine (*20, 21*). Most efforts to target nAChRs pharmacologically have been focused on developing direct agonists, antagonists, and allosteric modulators. However, given that nAChRs are found broadly throughout the nervous system, one major challenge to creating useful cholinergic drugs includes improving selectivity to target specific nAChR subtypes in particular regions of the brain. Another challenge is to avoid excessive activation of nAChRs which can result in cytotoxicity (*57, 58*). One way to circumvent these problems may be to target regulatory or auxiliary proteins that are able to modulate specific nAChRs.

In this study, we describe the opposing functions of two proteins that control nAChR assembly, NACHO and Ly6h. Using our flux assay, we showed that NACHO increases and Ly6h decreases the maximal response of α7 nAChRs in transfected HEK-tsa cells. The relative amounts of each regulatory protein determine the degree and valence of the overall effect. When both proteins are present, an intermediate response occurs that resembles the response when both proteins are absent. Previous studies have also shown that the chaperone Ric3 is able to synergize with NACHO to increase α7 currents (*40, 41*). However, in our flux assay, we did not observe any synergy between

NACHO and Ric3. Instead, the effect of NACHO seems to dominate over the effect of Ric3. It is worth noting that a limitation of our flux assay is that it has a sampling rate (4 s^{-1}) much slower than the kinetics of the α7 receptor, which is characterized by high calcium permeability, rapid activation, and fast desensitization within several hundred milliseconds (*59, 60*) . In order to measure α7 activation we used the positive allosteric modulator PNU-120596, which has been shown to block receptor desensitization without directly competing with Ly6h (*35*). Therefore, our assay can only measure steady-state activation of α7 and is unable to detect any kinetic changes of the receptor. As such, our assay suggests that any possible synergy between NACHO and Ric3 is likely not due to an increase of functional receptors at the cell surface. Further studies in both NACHO and Ric3 will be needed to investigate the mechanisms of synergy, if any, in regulating α7 nAChRs.

Additionally, we found that NACHO is able to decrease the EC_{50} of α7 nAChRs to agonists, despite NACHO remaining resident in the ER. We hypothesize that this reduction in the EC_{50} is results from NACHO displacing Ly6h or, in the absence of the latter, a functionally equivalent endogenous Ly6 protein that would otherwise travel with α7 subunits to the membrane to antagonize receptor activation. To test this hypothesis, we developed a functional competition assay involving NACHO and Ly6h. Using this assay, we found that the presence of NACHO significantly reduced the amount of Ly6h that was able to interact with α7 subunits. Since one of the reported functions of NACHO is to accelerate the assembly of nAChRs (*40*), we tested whether Ly6h might have the opposite effect and reduce receptor assembly. Using a biotinylated α-

bungarotoxin, we immunoprecipitated only fully formed α7 pentamers and found that the amount of these receptors was drastically reduced in the presence of Ly6h but enhanced by NACHO, with the sum of the two effects canceling out when Ly6h and NACHO were both present.

One possibility that may explain the underlying mechanism is that within the ER, free Ly6h may preferentially interact with α7 monomers. These Ly6h-α7 monomers would therefore be hindered in their ability to assemble into pentamers, resulting in a slower assembly rate than their unbound counterparts. If NACHO preferentially interacts with and assembles unbound α7 monomers into pentamers, this would mean that Ly6h essentially sequesters α7 monomers, forcing Ly6h-α7 monomers to be assembled via a separate, slower mechanism. As such, the α7 receptors at the surface of cells are likely to be a heterogeneous population—receptors that directly interact with Ly6h and those that do not. The antagonism between these NACHO and Ly6h may therefore represent a novel mechanism of regulation within the cell, which may help control endogenous cholinergic signaling in two ways, by 1) directly controlling the levels of α7 available at the cell surface, and 2) the probability of activation of the receptor population at the cell surface by modulating the proportion of Ly6h bound α7 receptors to unbound α7 receptors, resulting in receptors with differential EC_{50}. Given the important regulatory functions of NACHO and Ly6h, the endogenous expression levels of these two proteins are likely to also be tightly regulated, and fluctuations in the levels of these proteins, either induced pharmacologically or in pathological conditions, are likely to have significant downstream consequences. One recently published example shows that

perinatal nicotine exposure is able to increase NACHO protein levels in the rat frontal cortex in early postnatal development, but not in the hippocampus (*43*). The signaling that may lead to up or down-regulation of either NACHO or Ly6h in a temporal and spatial manner is largely unexplored. Given their antagonism with each other, however, these proteins may represent novel drug targets to correct aberrant nAChR signaling in pathological contexts.

In our present study, we also conducted a structure-function study on Ly6h, which is predicted to fold into a three finger (loops) motif, characteristic of the Ly6/ α-neurotoxin family of proteins. Despite a shared tertiary structure across all members of the Ly6 family, the only Ly6 protein with a solved structure is Lynx1 (*49*). To the best of our knowledge, no structure-function study has been conducted on any other mammalian Ly6 proteins. By systematically deleting each individual loop and subsequently deleting two loops at a time, while presumably conserving disulfide bonds, we identified loop 3 of Ly6h to be both necessary and sufficient for interacting with and inhibiting both α7 and α4β2 nAChRs. Loop 3 decreases the amount of receptor at the cell surface and consequently receptor-mediated currents, and it is also responsible for antagonizing the assembly of α7 nAChRs by NACHO. Given these effects, the corresponding peptide may provide structural insight into developing new pharmacophores to control nAChR signaling. For example, a synthetic peptide or a small molecule that either mimics or blocks loop 3 could allow α7 levels to be down or up-regulated, without directly inhibiting or activating the receptor itself. Although in this case selectivity may be hard to achieve since Ly6h has similar effects on α7 and α4β2 nAChRs, greater selectivity may

be achievable using a similar approach with any of the over 40 additional Ly6 proteins encoded in the mammalian genome, most of which have not been functionally characterized.

Interestingly, other Ly6 proteins have also been shown to modulate multiple effectors. For example, a *Drosophila* Ly6 protein named Sleepless (SSS) has been shown to modulate both nAChRs and a voltage-gated potassium channel named Shaker (*12, 61, 62*). Previous structure-function work in our lab has shown that both types of channels are regulated by the same loop of SSS (Chapter 2 (*50*)). Given the effects of single loops of both SSS and Ly6h, it is possible that other loops of both proteins interact with and modulate additional effectors. If this hypothesis is confirmed with Ly6h or any of its many homologs, different loops of Ly6 proteins may prove to be useful as novel peptide-based selective ion channel modulators in applications ranging from scientific research tools to potential therapeutic agents.

Figures

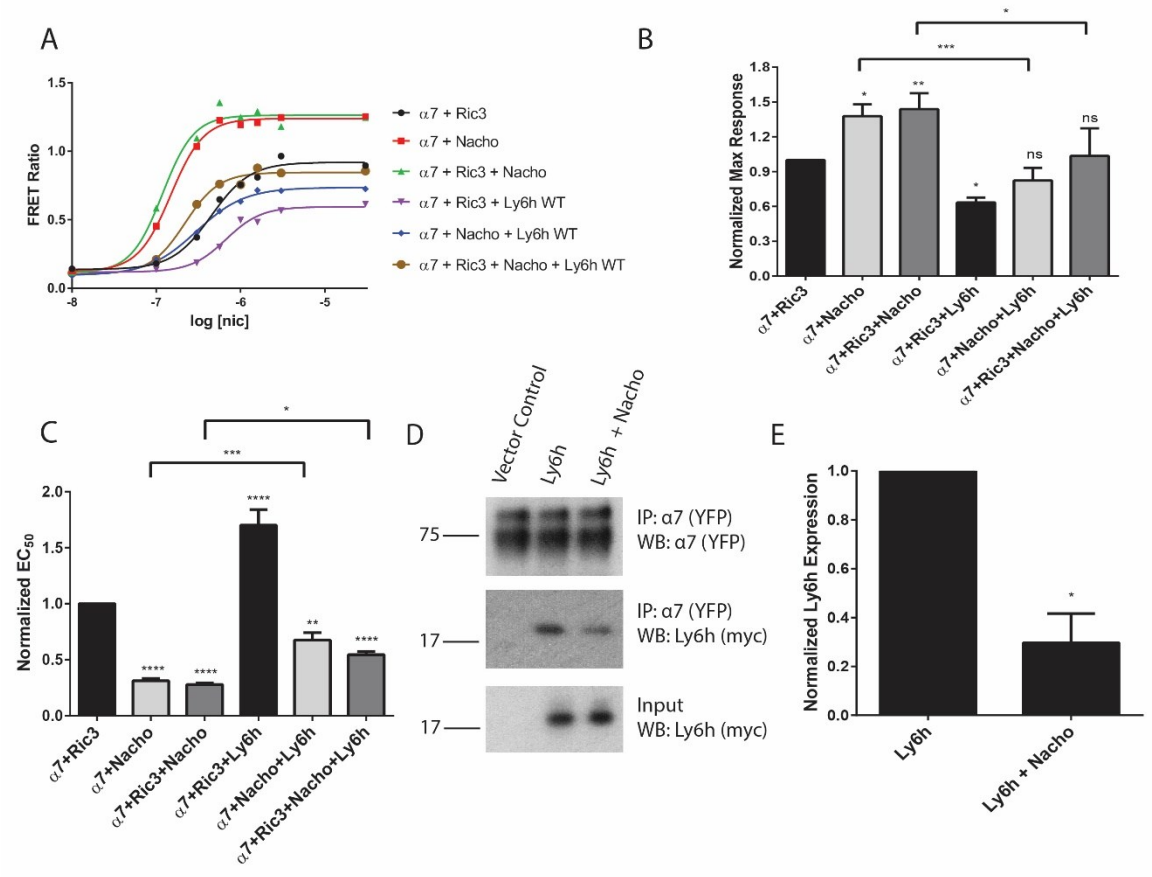

Figure 1- Direct antagonism between Ly6h and NACHO on α7 nAChRs. (A) Representative nicotine concentration-response curves of α7 either with or without NACHO, Ly6h, and Ric3 show that NACHO enhances and Ly6h suppresses the maximum response to agonist. (B) Average maximum response of α7 flux curves shown in A, normalized to α7 + Ric3 control (N>7). (C) Average EC_{50} of α7 flux curves shown in A, normalized to α7 + Ric3 control (N>7). (D) Representative co-immunoprecipitation blot of α7 showing a decreased Ly6h interaction with α7 in the presence of NACHO, despite equal levels in the input. (E) Average Ly6h protein levels co-immunoprecipitated with α7 in the presence of NACHO, quantified by pixel densitometry. Protein levels normalized to amount of Ly6h co-immunoprecipitated in the absence of NACHO (N=3). *p<0.05, **p<0.01, ***p<0.001, ****p<0.0001, and ns= not significant by one-way ANOVA and Dunnett's multiple comparisons test for B-C, and two-tailed T-test for E. Error bars represent standard error.

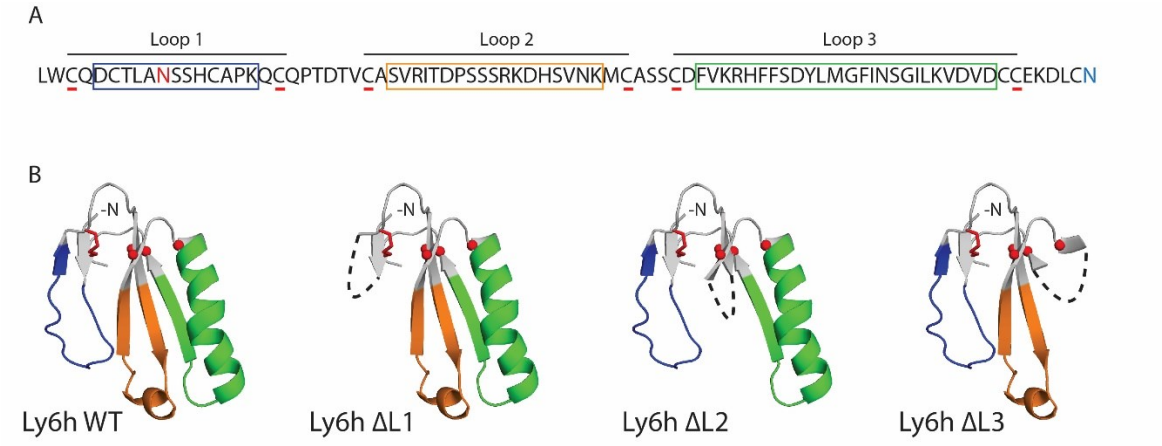

Figure 2- *De novo* structural prediction for Ly6h. (A) Amino acid sequence of Ly6h without the N-terminal signal sequence and the C-terminal GPI anchor. Conserved cysteines define the loop regions. Cysteines that are expected to participate in disulfide bond formation are underlined in red. Deletions were made to preserve one amino acid flanking the cysteines, as to not perturb disulfide bond formation. Deletion regions are represented by boxes. The predicted N-linked glycosylation site is at N56 in loop 1, as highlighted in red. The predicted GPI-anchor attachment site is predicted at N131 and is highlighted in blue. (B) *De novo* predictions by the software ROBETTA. Deleted regions which were replaced by a three alanine bridge are represented by dashed lines. Red sticks represent disulfide bond formation, while red spheres are conserved cysteines that are likely to form disulfide bonds, but were not predicted to by ROBETTA.

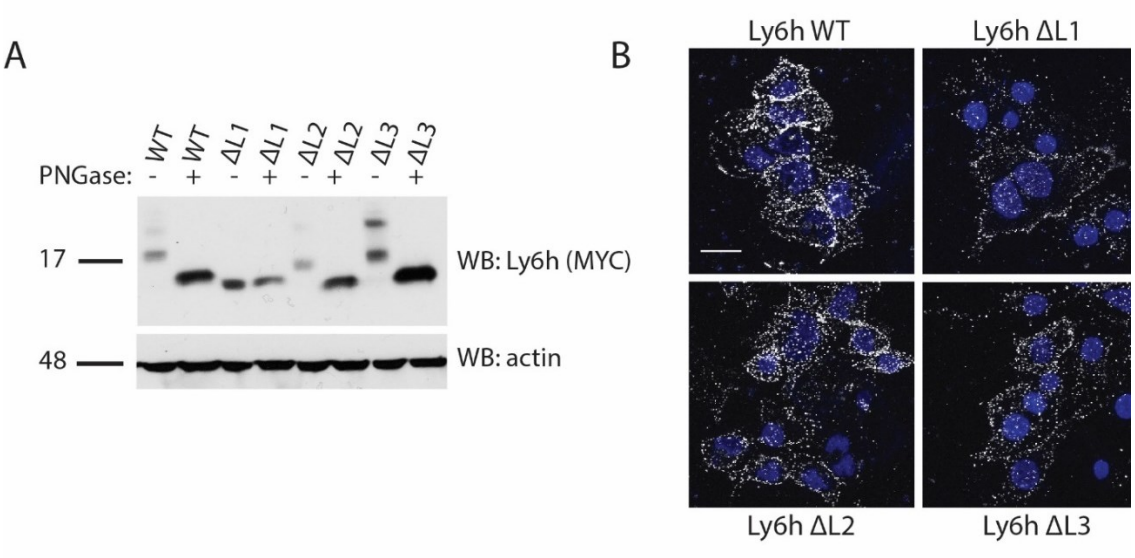

Figure 3- Ly6h mutants stably express, are glycosylated, and traffic to the plasma membrane. (A) Representative western blot of Ly6h and the loop deletion mutants. Higher molecular weight bands indicate the presence of glycosylated species. Incubation with PNGase-F collapses these bands. N>2 (B) Confocal imaging of Ly6h mutants under non-permeabilized conditions show that all mutants can be detected at the plasma membrane, indicating trafficking of these mutants is not abolished. Scale bar: 20μm. N=2

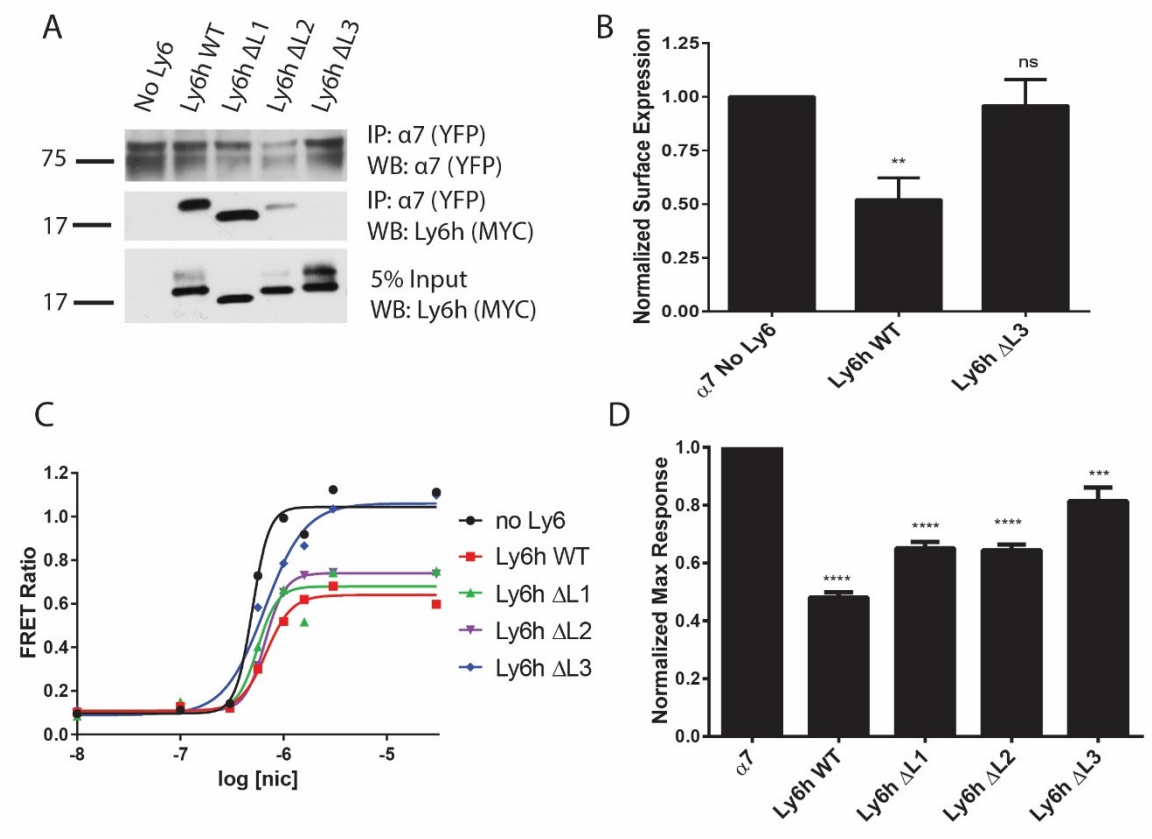

Figure 4- Loop 3 of Ly6h is required to interact with and functionally inhibit α7 nAChRs. (A) Representative blot of α7 immunoprecipitation with Ly6h loop deletion constructs. Loss of loop 3 abolishes the interaction between Ly6h and α7, despite being present in the input (N=6). (B) Summary of α7 surface expression levels in the presence of Ly6h and Ly6h ΔL3. Amount of surface receptor was determined by immunoprecipitating α7 subunits that contain an extracellular HA-tag. Surface protein levels quantified relative to total α7 levels and normalized to no Ly6h control. Loop 3 is necessary to decrease the amount of α7 present at the cell surface (N=7). (C) Representative nicotine dose-response curves of α7 activation in the presence of Ly6h loop deletion mutants. (D) Average maximal response of α7 flux curves seen in C, normalized to receptor alone controls. Loss of loop 3 greatly reduces the ability for Ly6h to inhibit α7 (N>6). **p<0.01, ***p<0.001, ****p<0.0001, and ns= not significant by one-way ANOVA and Dunnett's multiple comparisons test. Error bars represent standard error.

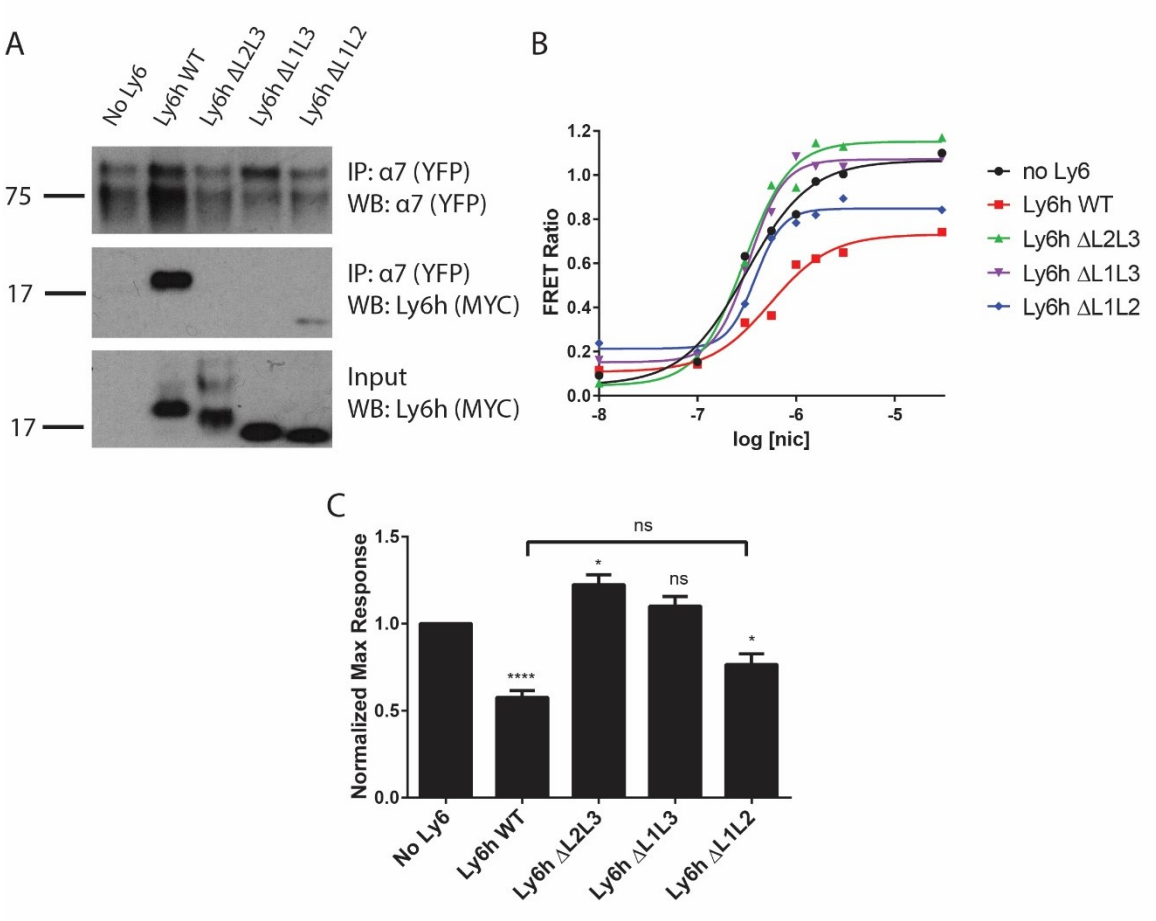

Figure 5- Loop 3 of Ly6h is sufficient to interact with α7 and inhibit α7 nAChR currents. (A) Representative blot of α7 immunoprecipitation with Ly6h double loop deletions. After immunoprecipitating α7, loop 1 alone (ΔL2L3) and loop 2 alone (ΔL1L3) are unable to be detected, despite being present in the total cell lysate input. However, loop 3 alone (ΔL1L2) is able to form a stable interaction with α7 and is immunoprecipitated with α7 (N=5). (B) Representative dose-response curve of α7 activation with Ly6h double loop deletion mutants. Ly6h ΔL1L2, which only consists of loop 3, is able to inhibit α7 mediated currents. (C) Average maximal response of α7 with Ly6h double loop deletion mutants, normalized to receptor alone controls. Loop 3 of Ly6h is sufficient to inhibit the maximal response of α7. N>7. *p<0.05, **p<0.01, ***p<0.001, ****p<0.0001, and ns= not significant by one-way ANOVA and Dunnett's multiple comparisons test. Error bars represent standard error.

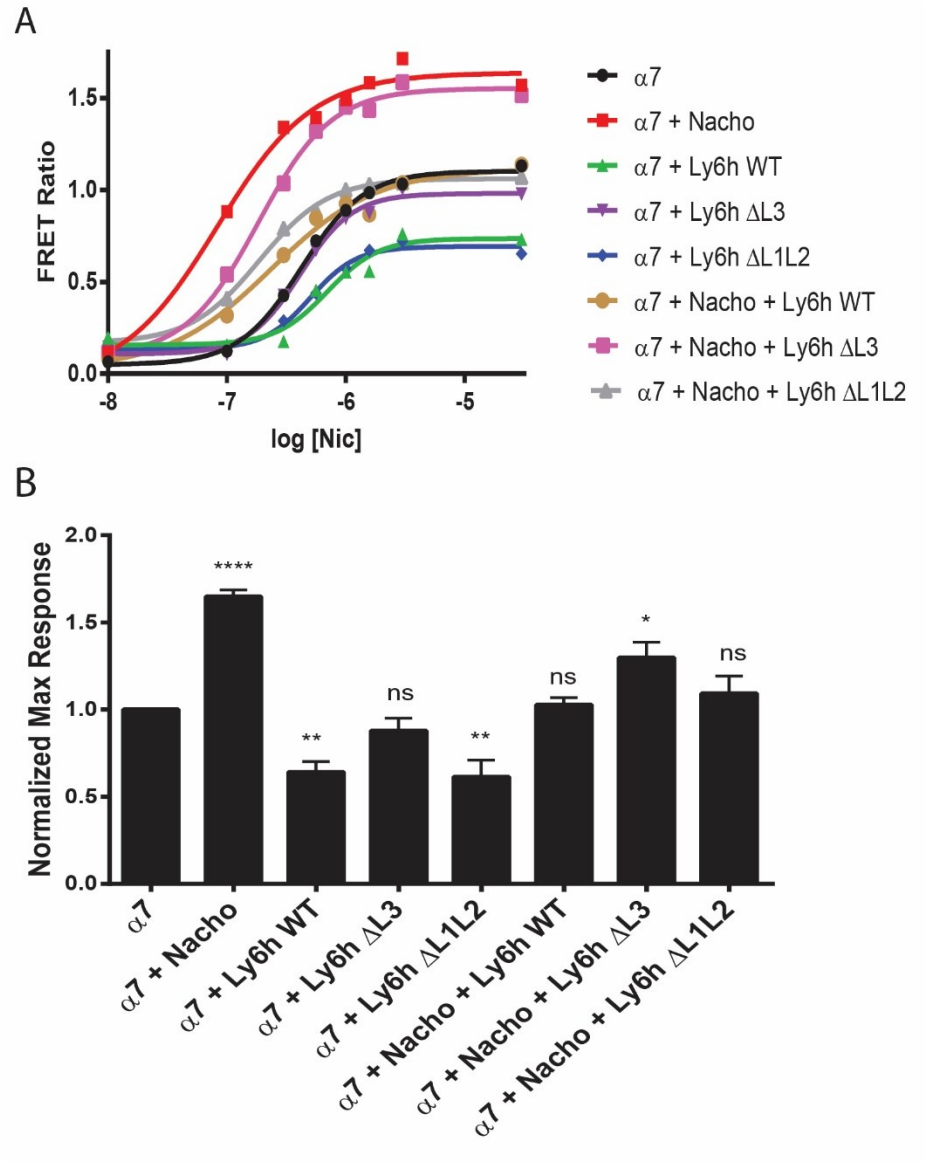

Figure 6- Loop 3 of Ly6h is necessary and sufficient to antagonize NACHO mediated increase of α7 currents. (A) Representative flux curve showing loop 3 of Ly6h is necessary and sufficient to functionally antagonize NACHO's effects on α7 fluxes. All conditions were run in the presence of Ric3. (B) Normalized maximum response of flux curves shown in A, normalized to control without Ly6h or NACHO (N=4). *p<0.05, **p<0.01, ****p<0.0001, and ns= not significant by one-way ANOVA and Dunnett's multiple comparisons test. Error bars represent standard error.

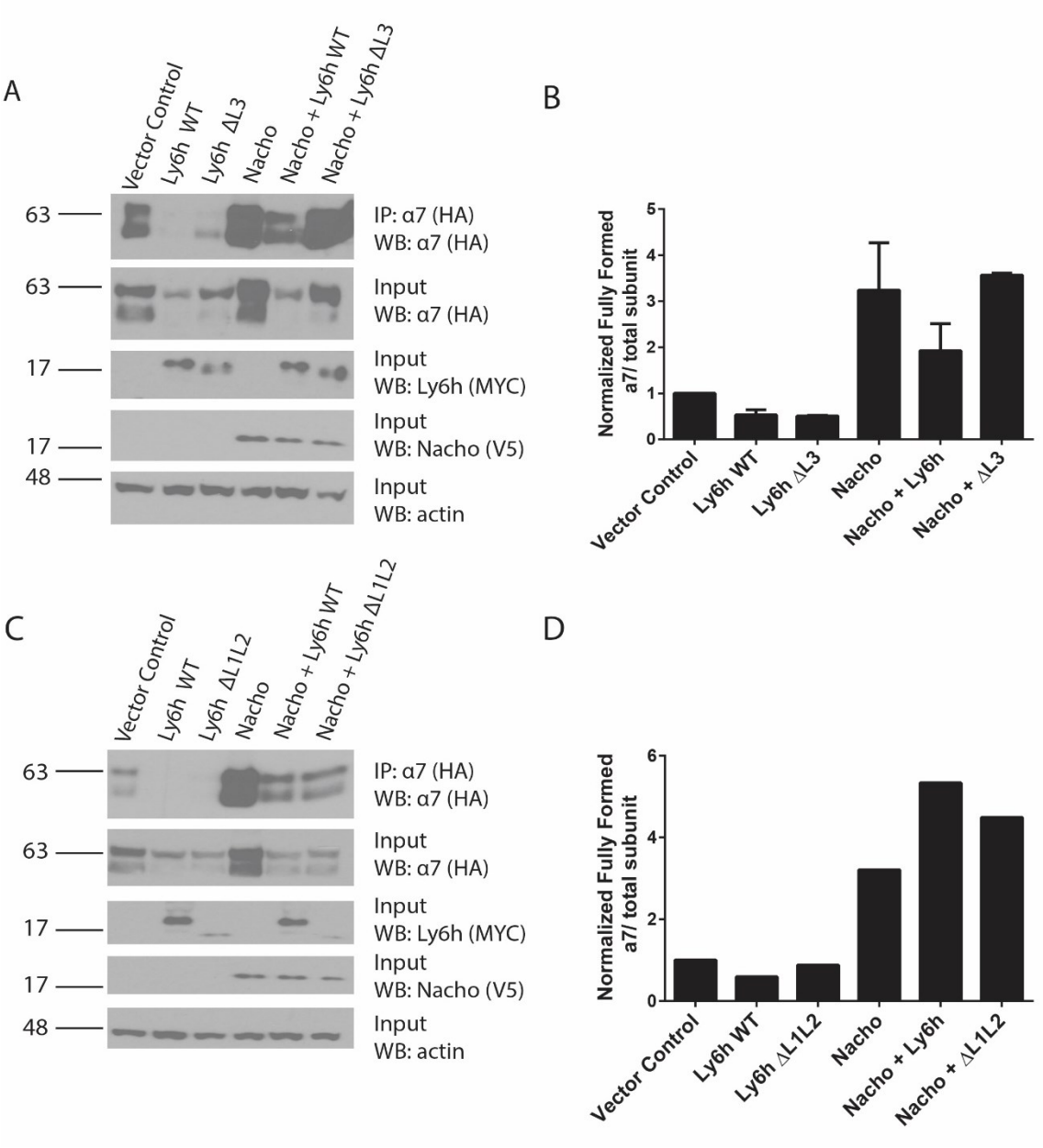

Figure 7- Loop 3 of Ly6h is necessary and sufficient to antagonize NACHO mediated assembly of α7 nAChRs. (A) Representative western blot of co-immunoprecipitation with α-bungarotoxin showing that Ly6h inhibits NACHO mediated assembly of α7 nAChRs. Deletion of loop 3 of Ly6h abolishes NACHO's effects on α7 assembly. (B) Summary of assembled α7 levels in A, relative to total α7 subunits and normalized to vector control, without Ly6h or NACHO (N=2). (C) Loop 3 of Ly6h is sufficient to antagonize NACHO mediated assembly of α7 nAChRs. (D) Quantification of C, relative to total α7 subunits and normalized to vector control (N=1). All conditions contain Ric3. Error bars represent standard error.

Supplemental Figures

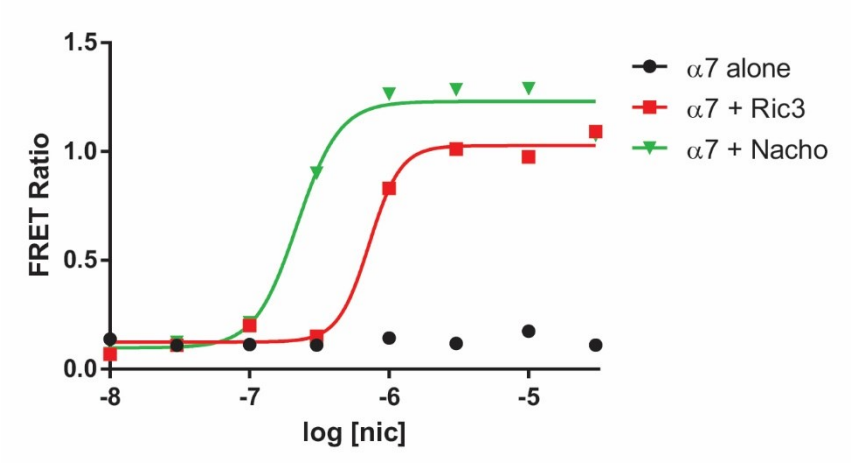

Figure S1- Either Ric3 or NACHO is required for functional heterologous expression of α7 nAChRs in HEK-tsa cells. HEK-tsa cells transfected with α7 alone does not produce any functional receptors, as detected by calcium-flux assay. Ric3 and NACHO alone are both able to form functional receptors in HEK-tsa cells.

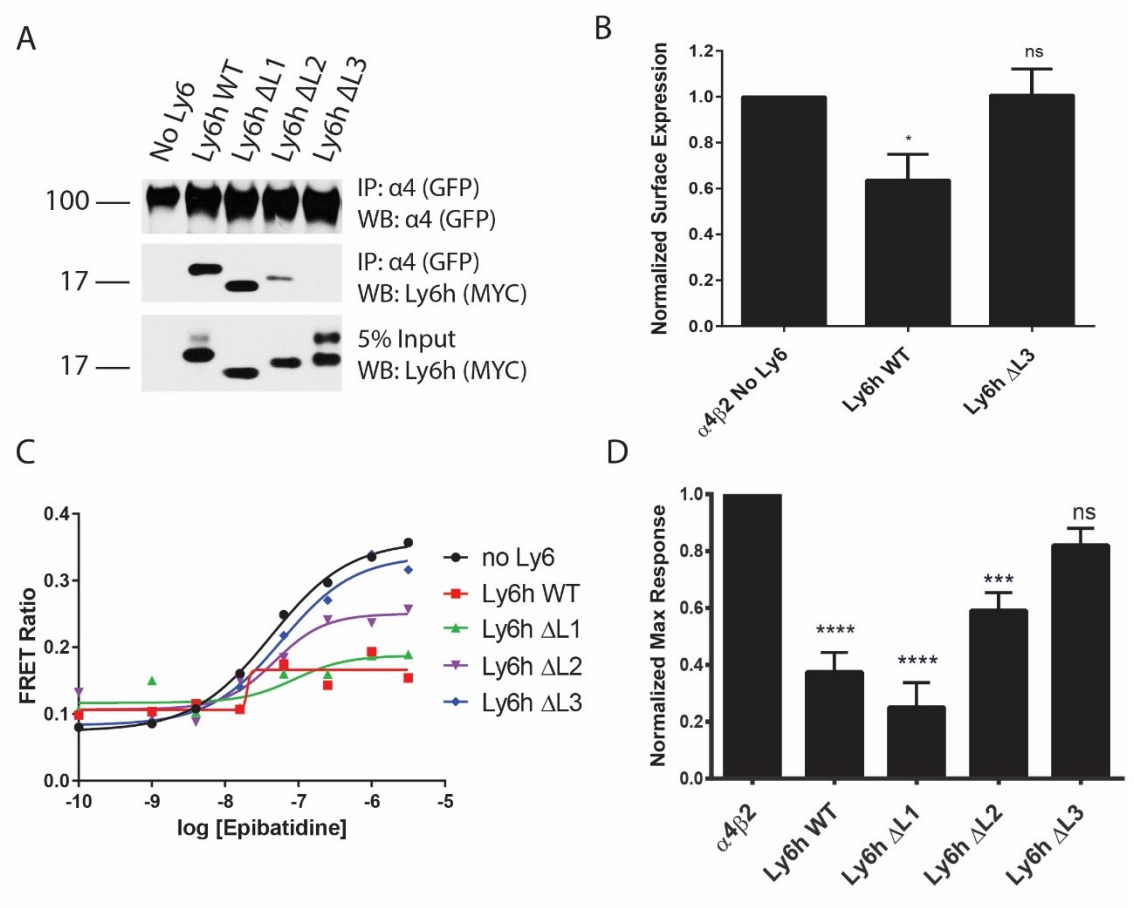

Figure S2- Loop 3 of Ly6h interacts with and inhibits α4β2 nAChRs. (A) Representative blot of α4β2 immunoprecipitation with Ly6h loop deletion constructs. Loss of loop 3 abolishes the interaction between Ly6h and α4β2, despite being present in the input (N=4) (B) Summary of α4β2 surface expression levels in the presence of Ly6h and Ly6h ΔL3, under chronic nicotine (1μM). Amount of surface receptor was determined by immunoprecipitating α4 subunits that contain an extracellular HA-tag. Surface protein levels quantified relative to total α4 levels and normalized to no Ly6h control. Loop 3 is necessary to decrease the amount of α4β2 present at the cell surface (N=11). (C) Representative nicotine dose-response curves of α4β2 activation in the presence of Ly6h loop deletion mutants. (D) Average maximal response of α4β2 flux curves seen in C, normalized to receptor alone controls. Loss of loop 3 greatly reduces the ability for Ly6h to inhibit α4β2 (N=4). *$p<0.05$, ***$p<0.001$, ****$p<0.0001$, and ns= not significant by one-way ANOVA and Dunnett's multiple comparisons test. Error bars represent standard error.

Chapter 2: Structural Analysis and Deletion Mutagenesis Define Regions of QUIVER/SLEEPLESS that Are Responsible for Interactions with Shaker-Type Potassium Channels and Nicotinic Acetylcholine Receptors

Introduction

Ly6 proteins are endogenous prototoxins found in most animals. They contain three short loops extending away from a hydrophobic scaffold that is anchored together by four conserved disulfide bonds (*49, 63, 64*). They belong to a superfamily of so-called "three-fingered" proteins that includes snake α-neurotoxins, which often interfere with ion channel function and cholinergic signaling pathways (reviewed in (*44*)). Similarly, Ly6 proteins have also been found to regulate ion channels and nicotinic acetylcholine receptors (nAChRs). One of the best-studied Ly6 proteins is SLEEPLESS (SSS; also known as QUIVER), found in *Drosophila*. Originally identified phenotypically in unmapped mutants that "quiver" in response to anesthesia and that exhibit reduced I_A currents (*65*), the gene encoding SSS was subsequently shown to be required for normal levels of sleep and mapped to the *quiver/sleepless* (*qvr/sss* or *sss*) locus (*12, 62, 66*). As its name suggests, loss of *sss* causes loss of sleep, much as in animals that have abnormally low levels of one of the protein's targets, the Shaker voltage-gated potassium (K) channel (*67*), or high levels of another target, Dα3 nAChRs (*12*). SSS has four primary effects on Shaker channels. It upregulates their protein levels (*12, 62, 66*); it accelerates their activation kinetics (*61*); it slows their C-type inactivation (*61*); and it speeds their recovery from inactivation (*68*). SSS also antagonizes nAChRs by unknown

means (*12*). The net result is that SSS acts as a suppressor of both excitability and cholinergic synaptic transmission (*12, 62, 66, 68*).

Like other single domain-containing members of the Ly6 family, SSS is highly processed post-translationally. Its N- and C-termini are both cleaved, and the remaining 98 amino acid protein is tethered to cellular membranes. SSS is also modified by N-linked glycosylation. The resulting sugar moiety is a common feature of many extracellular and intrinsic membrane proteins and is therefore unlikely to contribute to selective interactions between SSS and its target molecules. Instead selectivity is likely to be conferred by the protein-forming portion of SSS. How such selectivity is achieved is unknown, however, and is particularly intriguing considering that the small size of mature SSS limits the surface area through which protein-protein interactions can occur. To determine which protein motifs of SSS are required to form complexes with and regulate

K channels and nAChRs, we conducted a series of structure-function studies. We generated deletion mutants of SSS, expressed them heterologously, and assayed for co-immunoprecipitation with Shaker K channels and Dα3 nAChRs. We also tested whether each deletion mutant was able to suppress the activity of α4β2 nAChRs. Our data suggest that only loop 2 (i.e. the middle finger) of SSS is required for interactions with both classes of target molecules and for regulation of nAChRs. We also demonstrate that SSS normally inhibits nAChR activity by reducing levels of receptor at the cell surface, a process for which loop 2 is also required. Our data point for the first time to a structural motif required for a Ly6 protein to modulate effectors of neuronal activity. Such

information may be useful in design of Ly6 mimetics or antagonists with pharmacological utility in treating nervous system dysfunction in which cholinergic signaling plays a role.

Results

SSS Loop Deletions Produce Stable Proteins that Traffic to the Cell Surface

Like Lynx1, the only Ly6 protein whose structure has been solved (*49*), SSS is predicted to contain a single domain consisting of three short loops extending from a disulfide-rich hydrophobic core. As with other Ly6 proteins, SSS has also been shown to be anchored to the outer leaflet of the plasma membrane by glycosylphosphatidylinositol (GPI) and to be post-translationally modified by N-linked glycosylation (*66, 69-71*). Based on the consensus sequence for the latter type of modification, residue N57 in loop 1 is the most likely site for attachment of the sugar moiety (Fig 1A). Since the only published structural model of SSS is based on an algorithm that used the known structure of an α-neurotoxin as a primer (*62*), we asked whether de novo analysis would support the existing model for SSS. Using the computer program ROBETTA, which employs lowest free energy analysis, we generated an unbiased model of the tertiary structure of SSS that resembles the general structures of other three-fingered proteins (Fig 1B). The only deviation from these other structures is a pair of closely apposed but unbonded cysteines at the position in our model where a conserved disulfide bond is found in other three-finger proteins. Since disulfide bonds normally separate the core from the loops of

three-finger proteins, we used the predicted disulfide bonds in our model and the two unpaired cysteines described above to define the beginning of each loop of SSS. We then individually deleted each loop, leaving intact each disulfide-participating cysteine (or similar positions in loop 3) plus one flanking amino acid, and reconnected each exposed end with a three-alanine bridge (Fig 1B). We named these mutants SSS-ΔL1, SSS-ΔL2 and SSS-ΔL3. For each mutant we also made duplicate constructs in which we added a C-terminal MYC epitope. Because subsequent Western blot analysis showed that SSS-ΔL1 expressed poorly (data not shown), we generated two additional deletions that together encompassed all of loop 1, called SSS-ΔL1K1 and SSS-ΔL1K2. The interface between these smaller deletions was defined by an additional predicted disulfide bond, which was preserved in both new mutants (Fig 1B). Western blot analysis of cell lysates from transiently transfected HEK-tsa cells demonstrated that MYC-tagged SSS-ΔL1K1, SSS-ΔL1K2, SSS-ΔL2 and SSS-ΔL3 produce stable proteins (Fig 2A) at similar levels. Average normalized protein levels over several experiments confirm roughly similar expression levels (Fig 2B). These results support our structural predictions since gross misfolding would be expected to accelerate protein degradation. Furthermore, deglycosylation with PNGase-F (Fig 2A) resulted in the collapse of higher molecular weight bands to lower molecular weight bands, except in the case of SSS-ΔL1K2. We thus conclude that except for SSS-ΔL1K2, which is predicted to lack the sugar moiety of the other constructs, all the loop deletion mutants as well as wild-type SSS (SSS-WT) are modified by N-linked glycosylation. To test for proper protein folding of each mutant in more detail, we asked whether intracellular trafficking to normal membrane destinations was preserved. To address this question we immunostained HEK-tsa cells transiently

transfected with MYC-tagged SSS-WT or MYC- tagged loop deletion mutants. Transfected cells were stained with antibody in both non-permeabilizing and permeabilizing conditions, then fixed and imaged by confocal microscopy. Immunostaining of non-permeabilized cells demonstrated that, as previously described (*66*), wildtype SSS is accessible to antibody on the outside of the cell, as would be predicted for a GPI-anchored protein (Fig 2C; Fig S1). Furthermore, all of the loop deletion mutants except SSS-ΔL1K2 showed similar expression under the same conditions. Despite the low levels of SSS-ΔL1K2 seen at the cell surface, when transfected cells were permeabilized prior to antibody staining, SSS-ΔL1K2 was present at detectable, although slightly lower levels within the cell. Thus, except for this construct, all mutants undergo normal intracellular trafficking, suggesting that most deletions do not grossly disrupt the structure of SSS.

Loop 2 of SSS Is Required for Interactions with Shaker and Dα3

Our previous work demonstrated that SSS has a bi-functional role in regulating sleep in *Drosophila*. SSS forms complexes with the Shaker potassium channel and upregulates its levels, activation kinetics and avoidance of C-type inactivation (*62, 66, 68*). SSS also forms stable complexes with the Dα3 nAChR and suppresses nAChR function (*12*). Collectively, these regulatory processes are thought to suppress excitability and cholinergic synaptic transmission in wake-promoting neurons, thus facilitating sleep in flies. Using our loop deletion mutants, we examined which structural domain(s) of SSS might be involved in interactions with Shaker and Dα3. To address this question we first

transiently co-transfected Cos-7 cells with SSS-WT and either GFP-tagged Shaker or HA-tagged Dα3 cDNAs. We then immunoprecipitated tagged channel/receptor and Western blotted for the presence of SSS. As previously reported, we found that wildtype SSS forms stable complexes with both Shaker and Dα3 (Fig 3A and 3B; S2A and S2B). Next we tested which loops of SSS are required for these interactions. We found that SSS-ΔL1K1, SSS-ΔL1K2, and SSS-ΔL3 loop deletion mutants also co-immunoprecipitate with both Shaker and Dα3 to a similar extent as wildtype, with the exception of a slightly lower level for SSS-ΔL1K1 with Shaker. However, deletion of loop 2 (SSS-ΔL2) abolished interactions with both target molecules (Fig 3A and 3B; S2A and S2B). These results indicate that only loop 2 is necessary for SSS to maintain a stable complex with either Shaker or Dα3.

Loop 2 of SSS Is Required for Functional Inhibition of nAChR Activity

In addition to forming stable complexes with nAChRs, SSS inhibits nAChR activity (*12*). To determine if the same part of the SSS protein that facilitates complex formation with nAChRs also facilitates functional regulation of nAChRs, we used the ratiometric FRETable calcium reporter TN-XXL to measure calcium influx following activation of mouse α4β2 nAChRs. We used these receptors for our functional assays because Drosophila nAChRs have not produced robust currents alone in heterologous systems. Measurement of FRET ratios in HEK-tsa cells co-transfected with α4β2 and TN-XXL after stimulation with increasing concentrations of the nAChR agonist epibatidine resulted in an expected concentration-response relationship for receptor

activation (Fig 4A, black curve). As previously reported (*12*), addition of SSS-WT to transfection mixtures led to a decrease in the maximal response to agonist (Fig 4A, blue curve). Co-expression of all the loop deletion mutants except SSS-ΔL2 also resulted in inhibition of α4β2 activity (Fig 4A, pink curve; Fig 4B). Thus, similar to the structural requirements for interactions of SSS with its known targets, only loop 2 of SSS is necessary for functional inhibition of nAChR activity.

Loop 2 of SSS Is Required to Reduce Levels of α4β2 nAChRs at the Cell Surface

Like SSS, select mammalian Ly6 proteins have been shown to form complexes with and inhibit nAChR function. Various mechanisms have been proposed to account for the latter effect, including suppressed accumulation of nAChRs at the cell surface (*35, 36*). To determine if SSS similarly inhibits α4β2 nAChRs by regulating intracellular trafficking, we measured the amount of α4 subunit at the cell surface in the absence or presence of co-expressed SSS. HEK-tsa cells were transiently transfected with HA-tagged α4 and β2, and receptors at the cell surface were labeled with anti-HA antibody prior to cell lysis. Subsequent analysis of the labeled fraction of α4 subunits showed a small but detectable amount of receptor at the cell surface (Fig 5A, lane 1). We also found that surface expression of α4β2 nAChRs was potentiated by pre-incubation of the transfected cells for 20 hrs with the known chaperone, nicotine (1 μM), (Fig 5A, lane 4) as previously described (*17, 36, 72, 73*). Interestingly, co-expression of SSS-WT substantially reduced the amount of α4 detected at the cell surface, regardless of nicotine pre-incubation (Fig 5A and 5B). These results strongly suggest that like Lynx2 (*36*), SSS

reduces the maximal response of α4β2 nAChRs to agonist stimulation by limiting the availability of nAChR subunits at the cell surface. In contrast, SSS-ΔL2 did not affect surface α4 levels either in the presence or absence of nicotine pre-incubation (Fig 5A and 5B). Since the SSS-ΔL2 mutant reaches the cell surface on its own, our results thus suggest that loop 2 is required to form a complex with α4β2 nAChRs and thus to retain these receptors inside the cell away from activating agonist.

Discussion

The importance of Ly6 proteins is underscored by their implication in diseases such as Mal de Meleda (*47, 74, 75*); in nervous system functions such as synaptic transmission, visual plasticity, anxiety, and sleep (*9, 12, 35, 76*); and in immune and stem cell functions (*45, 70, 75, 77-82*). In some of these cases individual Ly6 proteins have been shown to exert their effects through antagonism of nAChRs, but the mechanisms underlying these effects and the structural motifs that are involved have not been thoroughly investigated. In this study, we examined the contributions of each of three loops of the Drosophila Ly6 protein SSS to complex formation with K channel and nAChR effectors, to regulation of nAChR activity, and to trafficking of nAChRs. Using a de novo structural model of SSS based on lowest free-energy folding predictions we identified disulfide bonds that appear to define the first two loops or "fingers" of SSS. This de novo model fell just short of predicting the formation of a third disulfide bond at the base of the third loop, despite the presence of conserved cysteines at the appropriate locations. This suggests that although our model is similar to known three-finger

structures, some differences do exist, and empirical measurements of the actual structure of SSS will be necessary to validate our predictions. Our analysis also predicted an additional disulfide bond in the first loop, thus suggesting that SSS structurally resembles non-conventional three-finger toxins, which do not show strong toxicity (reviewed in (*44*)). We used PCR-based mutagenesis to delete each loop individually as well as to generate two partial, complementary deletions in loop 1. We hypothesized that by leaving the disulfide-rich hydrophobic core of the protein intact we might be able to maintain the stability of each deletion mutant and thereby investigate the contribution of each loop to SSS function. This hypothesis appears to be generally correct. Although the deletion of loop 1 did not form stable protein, we observed stable expression of the remaining mutants, including those with smaller deletions in loop 1 (Fig 2A), suggesting that most mutants were not grossly misfolded or degraded. This hypothesis was reinforced by the PNGase-sensitive migration speeds of each mutant except for SSS-ΔL1K2, which lacked the predicted glycosylation site (Fig 2A), as well as by the detection of all mutants except SSS-ΔL1K2 at the cell surface (Fig 2B). Collectively these data suggest that most deletions do not impair protein stability or trafficking through the secretory pathway from the ER to Golgi to the plasma membrane. These results also validate the general predictions of our structural model for SSS. Despite the reduction of SSS-ΔL1K2 expression at the cell surface, this deletion mutant as well as the SSS-ΔL1K1, and SSS-ΔL3 mutants are still capable of forming stable complexes with both Shaker and Dα3 (Fig 3) as well as functionally inhibiting α4β2 nAChR activity (Fig 4). Instead, our data indicates that only loop 2 of SSS is necessary for interactions with both channel types and for regulation of α4β2 activity. Interestingly, loop 2 of α-cobratoxin and α-bungarotoxin

have been shown to interact with the ligand-binding pockets of acetylcholine binding protein (*83*) and α1 nAChRs (*84*), respectively. Thus, our data is consistent with the middle "finger" of three-finger proteins being particularly important for forming complexes with and regulating target molecules. Indeed, molecular modeling and site-directed mutagenesis suggest that the mammalian Ly6 protein Lynx1 interacts with the acetylcholine binding protein via residues at the tip of loop 2 (*49, 85*). However, it is somewhat surprising that the same structural element of SSS is responsible for complex formation with both nAChRs and K channels, since these target proteins have very different structures. While nAChRs have large extracellular ligand binding domains with which to interact with Ly6 proteins (*86*), crystal structures of potassium channels reveal very little protein surface exposed on the outer leaflet of the plasma membrane (*87*) or its topological equivalent in the vesicular sorting pathway. The shared requirement of loop 2 for interactions with multiple effector molecules has interesting implications for neuromodulatory functions of SSS. For example, it might be expected that a single molecule of SSS would be available to interact with a single K channel or nAChR but not with both simultaneously. This mutually exclusive interaction might hint at a mechanism by which SSS could co-regulate Shaker and Dα3, perhaps acting as a feedback "sensor" of the amount of either channel that is expressed or activated. Alternatively, it is possible that SSS, like some homologous snake α-neurotoxins, might form homodimers (reviewed in (*44*)) capable of interacting with two effector molecules simultaneously in a tetrameric complex. Further studies will be necessary to determine the likelihoods of both possible scenarios. Finally, our data reveal a conserved mechanism by which SSS inhibits nAChR function. As we previously showed for the mammalian Ly6 proteins, Ly6h and Lynx2

(*35, 36*), SSS appears to alter trafficking of nAChRs to reduce receptor levels at the cell surface, thus making them unavailable for activation by agonist (Fig 5). Interestingly, as we also showed for Lynx2 (*36*), this effect supersedes the ability of nicotine to chaperone α4β2 nAChRs. For SSS, however, we have gone one step further and shown that loop 2 is required to suppress nicotine's trafficking effects. One possible interpretation of this data is thus that loop 2 outcompetes intracellular nicotine for binding to α4β2 nAChRs. If this were the case then it would also suggest that Ly6 proteins exert some of their regulatory effects by interacting with the agonist-binding site of nAChRs. Such a mechanism would also account for how the SSS-ΔL1K2 mutant, which does not express well at the cell surface, can still interact with and inhibit α4β2 function, since such effects could occur intracellularly. In conclusion, our data demonstrate both a conserved mechanism for regulation of nAChRs by Ly6 proteins and a structural basis for such modes of regulation. In particular our data suggest a model in which the middle "finger" of some Ly6 proteins interacts with the agonist binding site of nAChRs to regulate receptor trafficking and ultimately function. In follow-up studies it will be interesting to determine how modes of nAChR regulation attributed to Ly6 proteins such as trafficking, desensitization kinetics, agonist sensitivity and receptor subunit stoichiometry differ in terms of the underlying structural perturbations. Ultimately, potentially subtle differences may be useful in designing drugs with enhanced selectivity for certain nAChR-Ly6 combinations found in restricted regions of the brain and possibly even for specific receptor conformations.

Figures

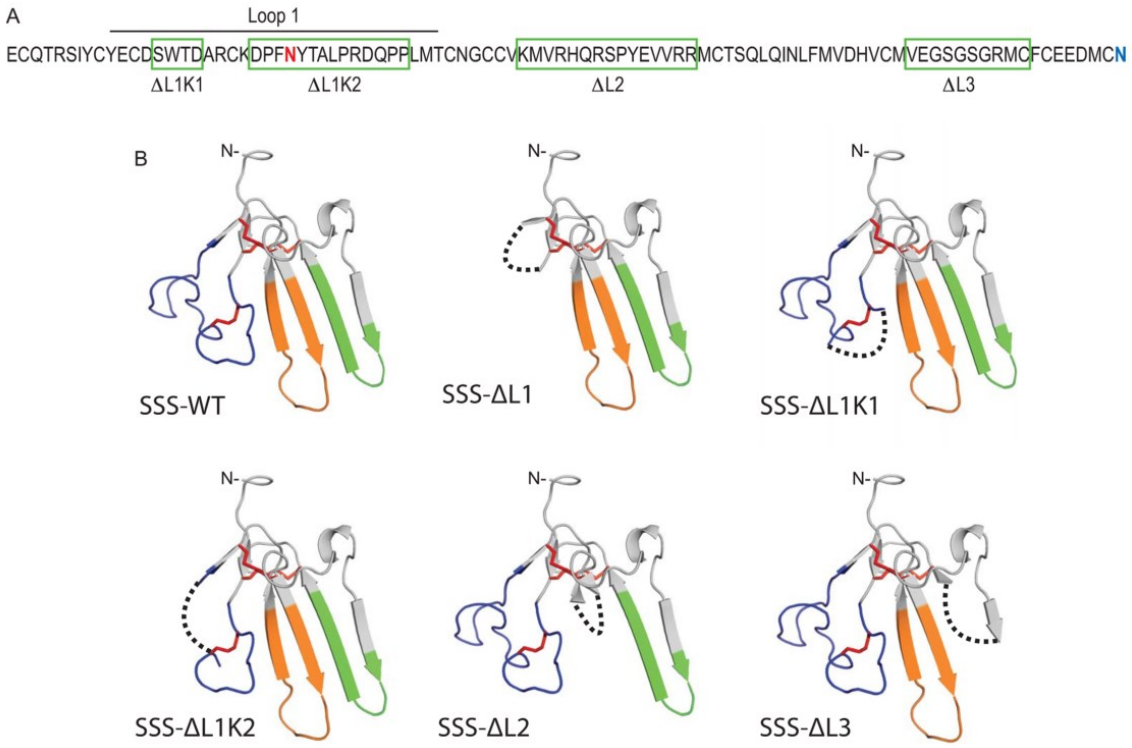

Figure 1- Structural modeling of SSS loop deletion mutants. (A) Amino acid sequence of SSS minus the predicted cleaved N- and C-termini. Loop deletions are designated by green boxes. Predicted N-linked glycosylation site (N57) is highlighted in purple and the predicted GPI-anchor attachment site (N127) is highlighted in light blue. (B) De novo Robetta model of SSS-WT. The N-terminus (after cleavage of the signal peptide) is marked accordingly. Red sticks indicate predicted disulfide bonds. Loop regions are denoted in navy (loop 1), orange (loop 2) and green (loop 3). For all panels, deleted protein segments are indicated with a dashed line.

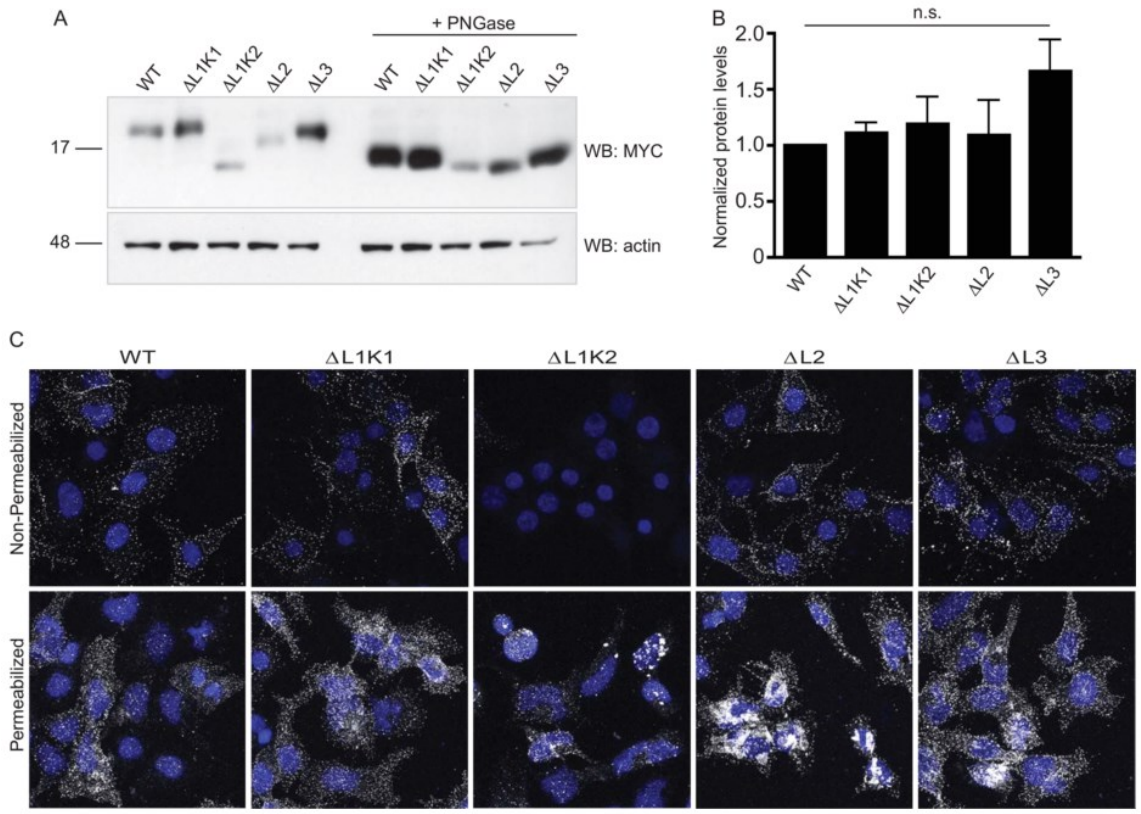

Figure 2- SSS loop deletion mutants are stably expressed and traffic to the plasma membrane. (A) Representative immunoblot of MYC-tagged SSS-WT and loop deletion mutants expressed in transiently transfected HEK-tsa cells. Left 5 lanes, untreated total cell lysates; Right 5 lanes, lysates treated with PNGase to remove N-linked glycosylation. Upper panel, immunoblot anti-MYC for SSS detection; bottom panel, immunoblot anti-actin for loading control. (B) Average normalized protein levels of SSS-WT and loop deletion mutants. Protein levels are not significantly different by one way ANOVA using Tukey's multiple comparison post-test. N = 4. (C) Representative immunostaining of HEK-tsa cells transiently transfected with MYC-tagged SSS-WT and loop deletion mutants. Upper panels: non-permeabilized cells show expression of all SSS proteins except ΔL1K1 at the plasma membrane. Bottom panels: permeabilized cells show total SSS expression.

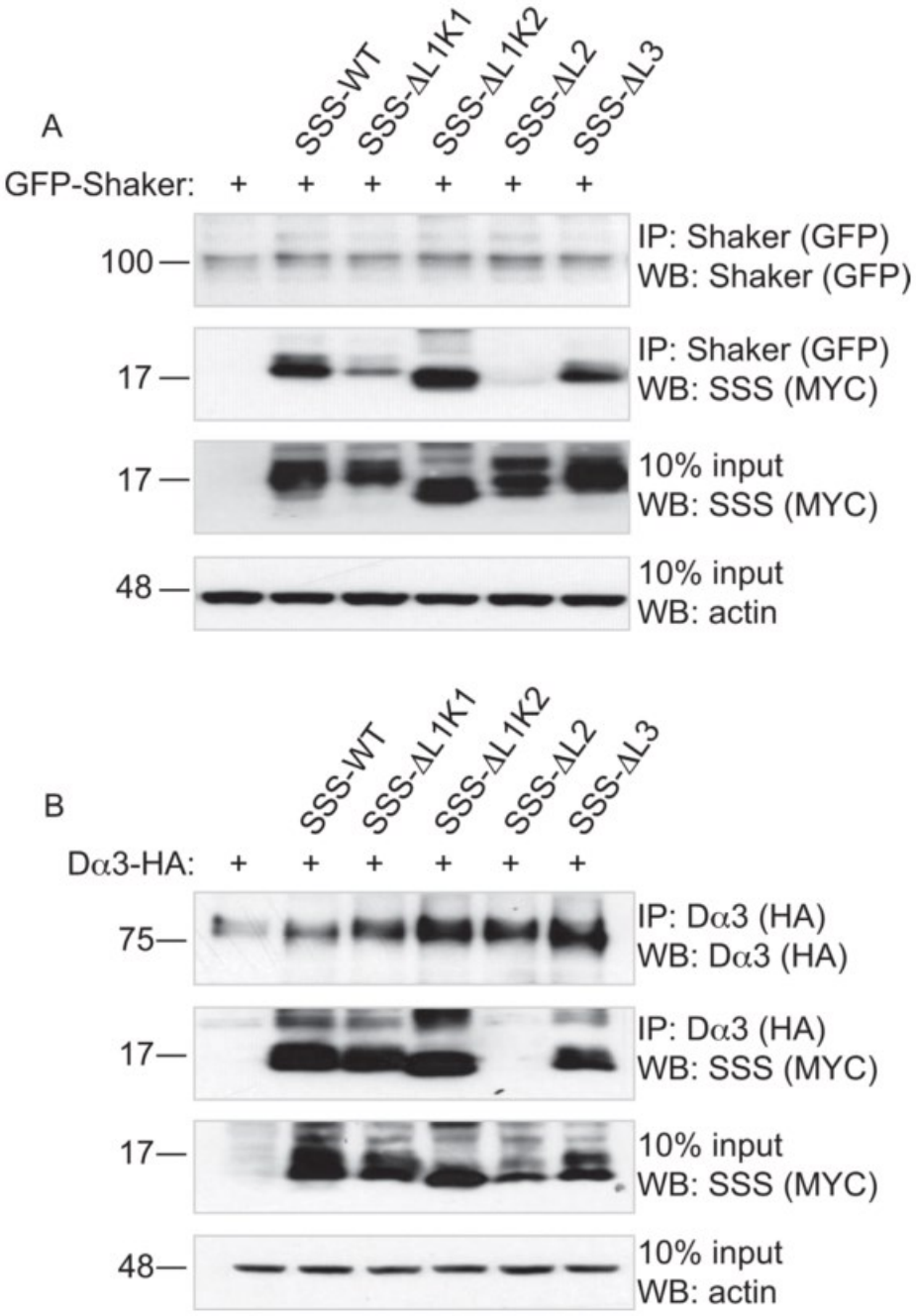

Figure 3- Loop 2 of SSS is required for complex formation with Shaker and Dα3 nAChRs. Representative immunoblots of complexes immunoprecipitated from Cos- 7 cells transiently transfected with: (A) GFP-tagged Shaker or B) HA-tagged Dα3, alone or with SSS loop deletion mutants. Top panels: IP-GFP (A) or IP-HA (B), immunoblot anti-GFP (A) or anti-HA (B). Second panels: IP-GFP (A) or IP-HA (B), immunoblot anti-MYC. Third panels: 10% input, immunoblot anti-Myc. Bottom panels: 10% input, immunoblot anti-actin.

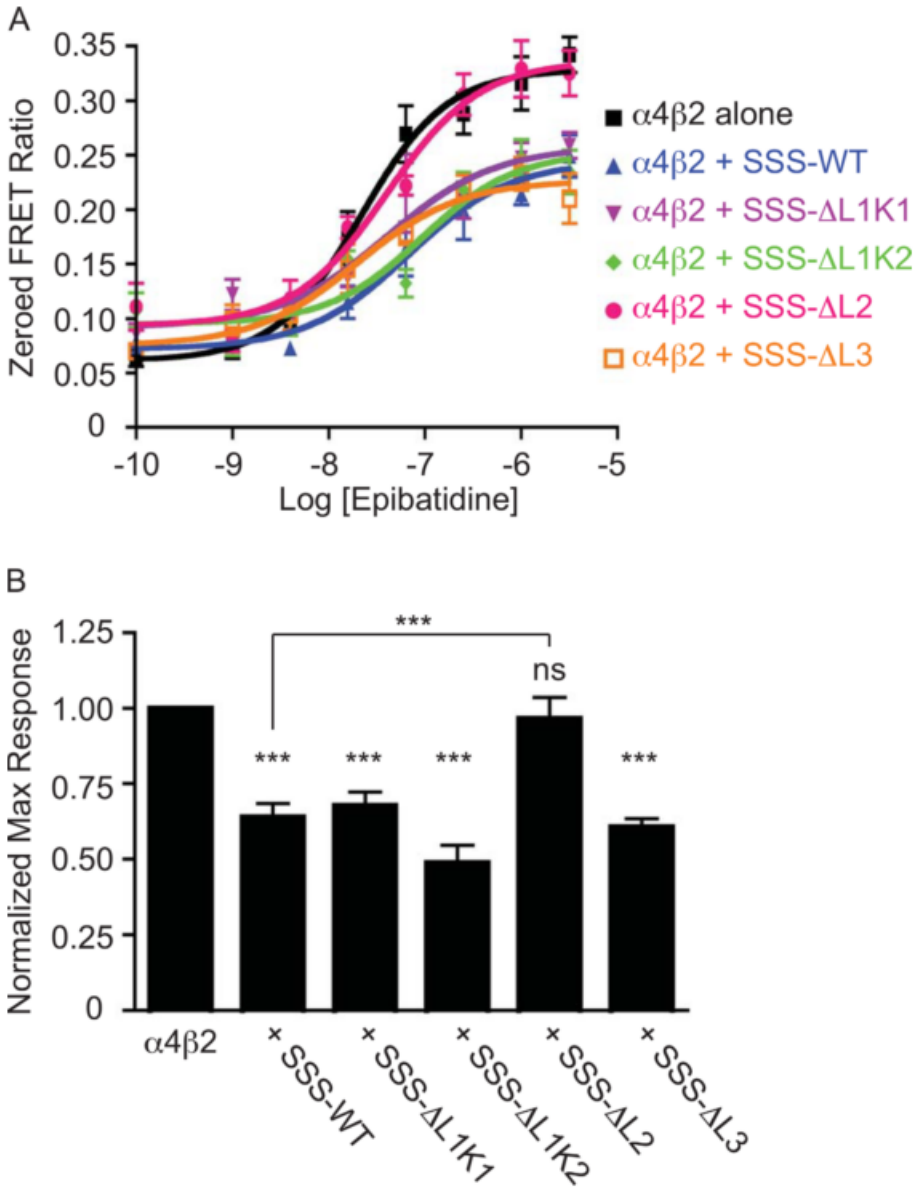

Figure 4- Loop 2 of SSS is required for inhibition of α4β2 nAChR activity. (A) Representative concentration-response curves for α4β2 activation by epibatidine alone (black line) or in the presence of SSS constructs (colored lines). (B) Average normalized maximum responses of α4β2 nAChRs to epibatidine alone or in the presence of SSS constructs (N>9). ***p<0.001 by one-way ANOVA and Tukey's multiple comparison post test. All stats are relative to α4β2 alone, except between SSS-WT and SSS-ΔL2, indicated by horizontal bar.

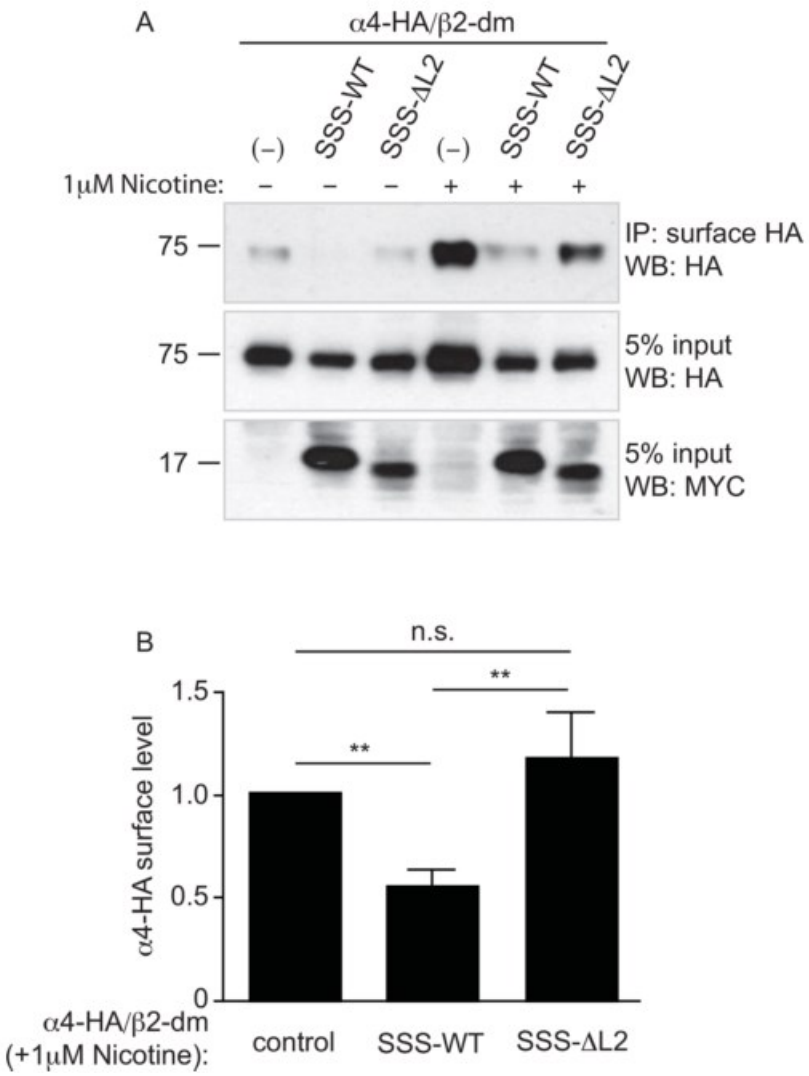

Figure 5- Loop 2 of SSS is required to reduce levels of α4β2 nAChRs at the cell surface. (A) Representative immunoblot of surface-labeled HA-tagged α4 immunoprecipitated from HEK-tsa cells co-transfected with untagged β2, alone or with SSS-WT or SSS-ΔL2. Lanes 4–6 are from cells that were pretreated with 1 μM nicotine for 20 hours to enhance trafficking of α4β2 to the cell surface. Upper panel: immunoprecipitated surface α4 HA, immunoblotted with anti-HA. Middle panel: 5%input, immunoblotted with anti-HA. Bottom panel: 5%input, immunoblotted with anti-Myc. (B) Average α4 HA surface levels (normalized to input) in nicotine-treated cells co-transfected with SSS constructs relative to no SSS control. N>6, **p<0.01 by one-way ANOVA and Dunnett's multiple comparison post-test.

Supplemental Figures

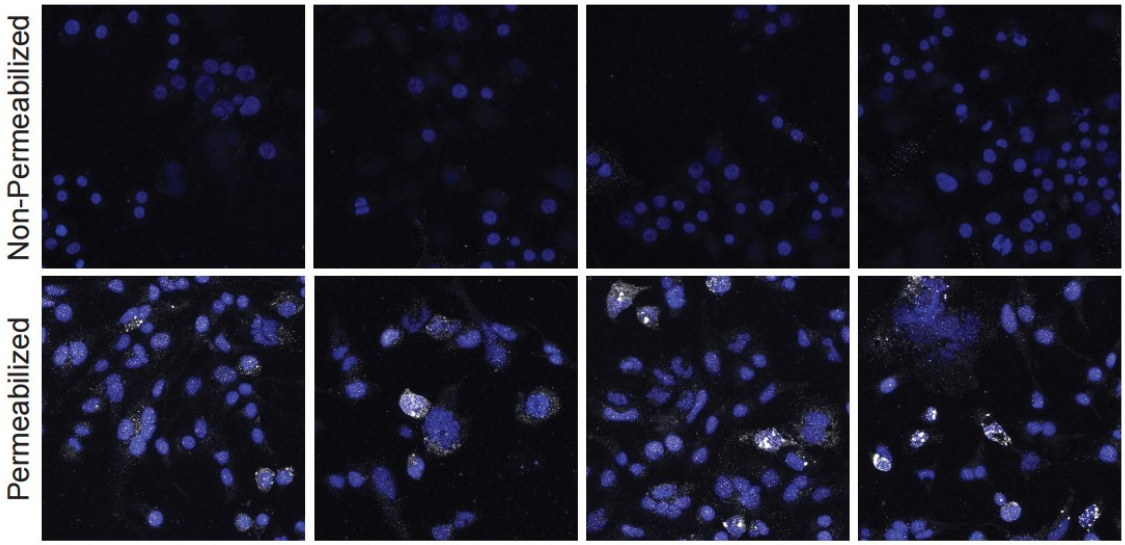

Figure S1- Deletion of SSS loop 2 allows for stable protein production but not for trafficking to the cell surface. This figure presents more examples of cell surface and intracellular staining of SSS ΔL1K2 to complement data in Fig 2c. All panels are from HEK-tsa cells transiently transfected with cDNA encoding SSS ΔL1K2. Top four panels are of SSS staining under non-permeabilizing conditions. No protein is apparent at the cell surface. Bottom four panels are of SSS staining under permeabilizing conditions. Protein is present inside cells.

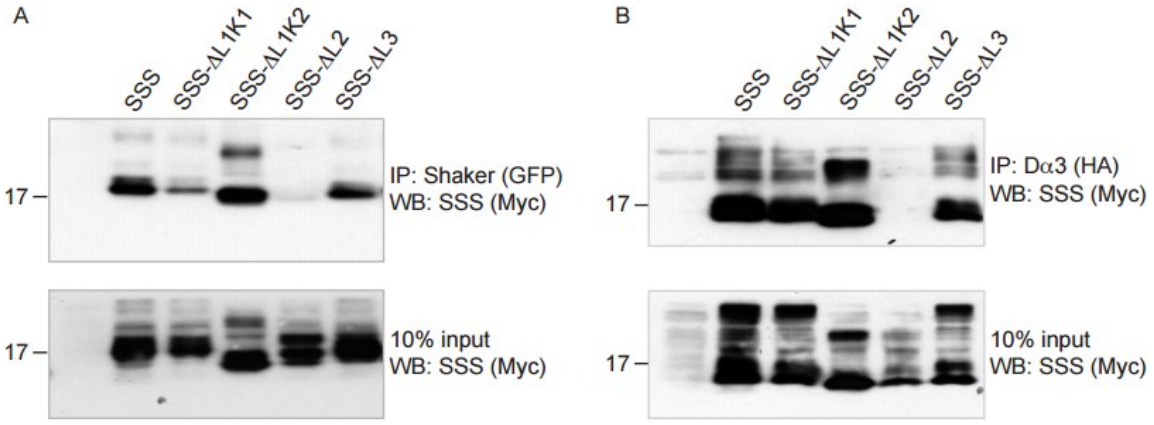

Figure S2- Full-length Western blots of SSS co-immunoprecipitation data from Fig 3. Top panels: MYC-tagged SSS loop deletions co-immunoprecipitated with GFP-tagged Sh (A) or HA-tagged Dα3 (B). Bottom panels: 10% input, immunoblot anti-MYC.

Chapter 2, in part, is a reprint of the material as it appears in PlosONE 2016. Wu, Meilin; Liu, Clifford Z.; Joiner, William J., PlosONE, 2016. I was the second author of this paper.

Future directions

As demonstrated throughout this thesis, various Ly6 proteins, such as Ly6h and SSS, are able to interact with and inhibit nAChR function. In particular, the mammalian protein, Ly6h, was able to antagonize NACHO, a protein that is believed to accelerate assembly of nAChRs and thus to significantly increase nAChR mediated currents in cells (*40, 41*). Given the antagonistic functions of these two proteins, it is possible that they contribute to the severity of certain pathological states for which nicotinic signaling has been implicated, such as Alzheimer's disease and nicotine addiction. It would be interesting to determine whether these proteins are pathologically up- or down-regulated, and to dissect the signaling cascade that might result in their transcriptional or translational regulation. For example, since Ly6h regulates Ca^{2+} influx through α7 nAChRs it may alter signaling through Ca^{2+}-activated enzymes including adenylyl cyclase and protein kinase A (PKA), PKC, Ca^{2+} -calmodulin dependent kinase II (CaMKII) and indirectly act on additional signaling pathways such as mitogen-activated protein kinase (MAPK) and the transcription factor cAMP response element-binding protein (CREB) (*5*). Of particular interest is the MAPK pathway, which has been shown to be activated by both nicotine and beta-amyloid protein via α7 nAChRs (*24, 25, 88*). Preliminary data in my lab suggests that Ly6h is downregulated in hippocampal pyramidal neurons following chronic exposure to Aβ in a manner that requires α7 activity. It would be interesting to see if this effect requires MAPK signaling by employing various pharmacological inhibitors, such as U0126, which blocks MEK1/2.

Furthermore, studies to understand how NACHO is affected via beta-amyloid may also help to understand the pathology of Alzheimer's.

In addition, it would be interesting to show that Ly6h is able to preferentially bind to unassembled α7 subunits, and that this binding directly impedes NACHO's ability to assemble pentamers. The flux data presented in Chapter 1 (Fig 1A), suggests that NACHO alone is sufficient to assemble pentamers, in the absence of Ric3. However, functional α7 pentamers requires the presence of either Ric3 or NACHO, since the absence of either results in no detectable α7 flux signal (Chapter 1, Fig S1). Given this, I hypothesize that Ly6h may preferentially bind to monomers of α7, and that this interaction impedes NACHO's function to assemble those monomers into pentamers. As such, the rate of assembly via NACHO will be slower if Ly6h is bound to α7 monomers, relative to unbound monomers. To determine if Ly6h affects the rate of assembly, it could be possible to perform a pulse chase experiment in HEK-tsa cells transfected with α7 and NACHO, with and without the presence of Ly6h. Upon labeling with 35S methionine, the amount of assembled receptor could be detected from total cell lysate with a biotinylated α-bungarotoxin. By analyzing the amount of α7 pentamers with the incorporated 35S methionine, it would be possible to determine the basal rate of assembly by NACHO, and whether this rate of assembly is decreased with Ly6h overexpression. This could point to the presence of Ly6h directly interfering with NACHO's function—one possibly could be that Ly6h imposes a steric effect on NACHO, or vice versa, that results in kinetic consequences. A heterologous expression system with HEK-tsa would probably be the best way to perform this experiment, since Ric3 is not normally found in

HEK-tsa cells (Chapter 1 Fig S1). However, this assay could potentially be done in cultured hippocampal neurons using a viral Ly6h shRNA, but the presence of Ric3 would complicate interpretation of the results.

Materials and Methods

Molecular Biology and DNA constructs

NACHO was cloned from mouse brain cDNA using the following primers, and then subcloned into a pcDNA3 vector with the restriction sites XhoI/ EcoRI:

NACHO-F (EcoRI): 5' GAC GAA TTC CCC ATG GCA TCC CCA CGA ACC ATA ACT ATC ATG G 3'

NACHO-R (XhoI): 5' CAA TTT CTC GAG TTA TGA CAC CTT CAC TTT GCC CTG 3'

A V5 tag was added to the N-terminus via PCR stitching, using the V5 tag from an existing V5_MC2R vector in pcDNA3 (gift from the J. Trejo Lab at UCSD). The following primers were used for stitching:

NACHO Stitch-F (HindIII): 5' CGA CTC ACT ATA GGG AGA CCC AAG CTT GG 3'

NACHO Stitch-R (XhoI): 5' GAA TAG GGC CCT CTA GAT GCA TGC TCG AG 3'

V5-tag Stitch-F: 5' GTG TGC TGG AAT TCC CCA TGG GTA AGC CTA TCC CTA ACC C 3'

V5-tag Stitch-R: 5' GTT ATG GTT CGT GGG GAT GCC GTA GAA TCG AGA CCG AGG 3'

Ly6h and SSS loop deletions were generated by QuikChange PCR mutagenesis of untagged Ly6h and SSS in pcDNA, along with MYC-tagged Ly6h and SSS in pcDNA (*12, 35*).

Ly6h mutants were created using the following primers:

ΔL1-F: 5’ GGC CTG TGG TGC CAG GCG GCC GCT CAG TGC CAG CCC ACC 3’

ΔL1-R: 5’ GGT GGG CTG GCA CTG AGC GGC CGC CTG GCA CCA CAG GCC 3’

ΔL2-F: 5’ CCA CCG ATA CCG TTT GTG CCG CGG CCG CTA TGT GTG CTT CCT CCT GCG A 3’

ΔL2-R: 5’ TCG CAG GAG GAA GCA CAC ATA GCG GCC GCG GCA CAA ACG GTA TCG GTG G 3’

ΔL3-F: 5’ GCT TCC TCC TGC GAC GCG GCC GCT TGC TGC GAG AAA GAT 3’

ΔL3-R: 5’ ATC TTT CTC GCA GCA AGC GGC CGC GTC GCA GGA GGA AGC 3’

Double loop deletion constructs were made using the same oligos as listed above, except with the original single deletion mutant constructs as a template.

SSS loop deletion mutants were created using the following primers:

ΔL1 F: 5’ CGC GAT CGA TTT ACT GCT ATG CGG CCG CTA CCT GCA ACG GTT GCT GCG T 3’

ΔL1 R: 5’ ACG CAG CAA CCG TTG CAG GTA GCG GCC GCA TAG CAG TAA ATC GAT CGC G 3’

ΔL1K1 F: 5’ TGC TAT GAG TGC GAC GCG GCC GCT CGC TGC AAG GAT CCT 3’

ΔL1K1 R: 5’ AGG ATC CTT GCA GCG AGC GGC CGC GTC GCA CTC ATA GCA 3’

ΔL1K2 F: 5’ GAT GCC CGC TGC AAG TTG ATG ACC TGC AAC 3’

ΔL1K2 R: 5’ GTT GCA GGT CAT CAA CTT GCA GCG GGC ATC 3’

ΔL2 F: 5’ AAC GGT TGC TGC GTG GCG GCC GCT ATG TGT ACG TCA CAG 3’

ΔL2 R: 5’ CTG TGA CGT ACA CAT AGC GGC CGC CAC GCA GCA ACC GTT 3’

ΔL3 (untagged) F: 5’ TGG TCG ATC ACG TGT GCA TGG CGG CCG CTT TTT GTG AGG AAG ATA TGT GC 3’

ΔL3 (untagged) R: 5’ GCA CAT ATC TTC CTC ACA AAA AGC GGC CGC CAT GCA CAC GTG ATC GAC CA 3’

ΔL3 (MYC tagged) F: 5’ TGG TCG ATC ACG TGT GCA TGG CGG CCG CTT TTT GTG AGG AAG ATA TCG AGC 3’

ΔL3 (MYC tagged) R: 5’ GCT CGA TAT CTT CCT CAC AAA AAG CGG CCG CCA TGC ACA CGT GAT CGA CCA 3’

cDNAs of α7-pcDNA3, hRIC3-pcDNA3, α4-pciNEO, β2-dm-pciNEO, YFP-tagged α7, and GFP-tagged α4 were gifts from H. Lester. Both YFP-tagged α7 and GFP-tagged have been shown to be functional receptors (*89, 90*). TN-XXL was a gift from P. Taylor. HA-tagged α4 was generated as previously described (*36*). HA-tagged α7 was generated similarly to that of HA-tagged α4. HA-tagged Dα3 and GFP-tagged Shaker were also generated as previously described (*12*).

De novo structural models were generated by submitting the FASTA sequences through Robetta Full-chain Protein Structure Prediction at http://robetta.bakerlab.org/. Robetta models were visualized using the free software PyMol (www.pymol.org). Sequence analysis for prediction of signal peptide and post-translational modifications were performed using algorithms found at http://www.cbs.dtu.dk/services/SignalP/, http://www.imtech.res.in/raghava/glycoep/submit.html, and http://mendel.imp.ac.at/gpi/gpi_server.html.

Cell Culture, Immunoprecipitations and Biochemistry

HEK-tsa cells ((*91*) via T. Hoshi lab, University of Pennsylvania) and Cos-7 cells (ATCC #CRL- 1651 via J. Trejo lab, UCSD) were maintained in growth media containing Dulbecco's modified Eagles media (DMEM, Mediatech) supplemented with 10% fetal bovine serum (Omega), 1% penicillin/streptomycin (Mediatech) and 1% L-glutamine (Sigma) at 37°C with 5% CO2. All experiments were performed using HEK-tsa cells, except Shaker and Dα3 co-immunoprecipitations, which were performed using Cos-7 cells. Cells were transfected using X-tremeGene HP (for HEK-tsa) or X-tremeGene-9 (for Cos-7) transfection reagent (Roche) as previously described (*35*). Cells were lysed in SDS lysis buffer [10mMTris, pH 7.5; 100mMNaCl; 5mM EDTA; 1% Triton X-100; and 0.05% SDS with cOmplete protease inhibitor (Roche)] and prepared for immunoprecipitation or Western blotting as previously described (*35*).

For co-immunoprecipitation experiments, rabbit anti-GFP antibody (0.2 µl/ml Life Technologies) was used for YFP-tagged α7, GFP-tagged α4, and GFP-tagged Shaker. Rabbit anti-HA (Rockland) was used for HA-tagged α7, α4, and Dα3. Co-immunoprecipitation was done as previously described (*35*). Immunoprecipitation of fully assembled α7 receptor was done with 100nM of biotinylated α-bungarotoxin (Biotium), left rotating overnight at 4°C in RIPA buffer [150mM NaCl; 25mM HEPES, pH 7.5; 1% Triton-X100; 0.1% SDS; and 1% sodium deoxycholate with cOmplete protease inhibitor (Roche)]. Streptavidin-conjugated agarose beads (Pierce) were then added and left on a rotating platform at 4°C for 4 hours. Streptavidin-agarose beads were washed three times in 1ml RIPA buffer and stored in 4x LDS sample buffer (Life

Technologies). For input conditions, 50µg of total cell lysate was loaded per lane. Immunoprecipitations were done with 500µg of total cell lysate. α4-HA and α7-HA surface labeling was performed as previously described (*36*) using rabbit anti-HA (0.6 µl/ml Rockland) antibodies. Briefly, cells were incubated for 1hr with rabbit-anti-HA antibody prior to lysis. Antibodies were washed off, and cells were lysed in SDS lysis buffer. 5% of total cell lysate was reserved for input sample, and the remainder was diluted in IP buffer [10mM Tris pH 7.5; 100mM NaCl; 0.5% Triton X-100; 0.05% SDS] and incubated with protein G magnetic beads for 4hrs at 4°C on a rotating platform. Western blot analysis was then run for the cell lysates and co-immunoprecipitation complexes. Densitometry analysis was performed to determine the ratio of receptor at the surface to amount of total nAChR monomer. Ratios were normalized to control, which was transfected with receptor alone, without any Ly6 proteins.

Rabbit anti-GFP (1:500, Life Technologies), mouse anti-HA (1:1000, Covance) and mouse anti-MYC (1:250, Santa Cruz Biotechnologies) were used for Western blotting. Peptide- N-Glycosidase F (PNGase F) treatment of cell lysates to remove glycosylation modifications were performed according to the manufacturer's instructions (PNGase, NEB) with the following modification: cOmplete Protease Inhibitor (Roche) was included during the enzymatic treatment (0.3 µl PNGase) which was performed for 2 hours at 37°C. PNGase-treated samples were run on a 12% gel (NuPage, Life Technologies) to maximize band separation at low molecular weight.

Immunostaining

HEK-tsa cells transiently transfected either MYC-tagged Ly6h-WT/ Ly6h-loop deletion mutants, or SSS-WT/ SSS-loop deletion mutants. Cells were stained 48hrs after transfection either before (non-permeabilized) or after (permeabilized) cell fixation with 4% Formaldehyde (Sigma). Staining was done with anti-MYC antibody (1:100, SantaCruz Biotechnology) in Optimem (Life Technologies) on ice for one hour. Permeabilized cells were incubated in 0.1% TritonX-100 and 0.1% deoxycholate solution in PBS for 1 minute at room temperature, immediately prior to staining. Coverslips were washed once with Optimem and incubated with Alexa Fluor Goat anti-Mouse 488 (1:600, Life Technologies) in 5% goat serum for 1 hour. Coverslips were washed three times in PBS and incubated with DAPI for 1 minute at room temperature. Coverslips were washed once more with PBS and mounted onto glass slides in 1.5 µl VectaShield (Vector Laboratories).

FRET-Based Measurements of nAChR Activity

HEK-tsa cells were transiently transfected with mouse cDNAs of α7 or α4β2 nAChRs. To test activity of α7 nAChRs, cells were transfected with α7, hRic3, and TN-XXL, with or without untagged Ly6h-WT/ Ly6h-loop deletion mutants, at a ratio of 1:1:2:5. To test activity of α4β2, cells were transfected with α4, β2-dm, and TN-XXL, with or without untagged Ly6h-WT/ Ly6h-loop deletion mutants, or SSS-WT/ SSS-loop deletion mutants. Cells were then prepared for FRET assay as previously described for α4β2 (*12*) and α7 (*35*). Briefly, 24 hours after transfection, cells were re-plated into black 96-well clear-bottom plates (Corning). Cells for α4β2 were pre-treated with 1 µM

nicotine (R&DSystems) for 20 hours. Growth media was replaced with artificial cerebrospinal fluid (ACSF: 121mM NaCl, 5mM KCl, 26mM $NaHCO_3$, 1.2mM $NaH_2PO_4H_2O$, 10mM Glucose, 5mM HEPES, either 3.4mM Ca^{2+} for α4β2 or 2.4mM Ca^{2+} for α7, and either 0.65mM Mg^{2+} for α4β2 or 1.3mM Mg^{2+} for α7 [pH 7.4]). Cells for α7 were supplemented with 10μM N-(5-chloro-2,3-dimenthoxylphenyl)-N' (5-methyl-3-isoxazolyl)-urea (PNU)-120596 in ACSF for 30 minutes prior to flux to block receptor desensitization. Cells were then assayed by stimulation with increasing concentrations of either nicotine or epibatidine (R&DSystems). Average maximum responses and EC_{50} were calculated from concentration-response curves, each performed in duplicate or triplicate, with results normalized to the maximum response of nAChRs without any Ly6 proteins. Curves with hillslopes <1.0 or >5.0 were excluded from analyses. One-way ANOVA repeated-measures analysis with Dunnett's multiple comparison post test was used for statistical analysis.

References

1. A. J. Thompson, H. A. Lester, S. C. R. Lummis, The structural basis of function in Cys-loop receptors. *Quarterly Reviews of Biophysics* **43**, 449-499 (2010)

2. V. Tsetlin, D. Kuzmin, I. Kasheverov, Assembly of nicotinic and other Cys-loop receptors. *Journal of Neurochemistry* **116**, 734-741 (2011)

3. C. Gotti, F. Clementi, A. Fornari, A. Gaimarri, S. Guiducci, I. Manfredi, M. Moretti, P. Pedrazzi, L. Pucci, M. Zoli, Structural and functional diversity of native brain neuronal nicotinic receptors. *Biochemical Pharmacology* **78**, 703-711 (2009)

4. R. Giniatullin, A. Nistri, J. L. Yakel, Desensitization of nicotinic ACh receptors: shaping cholinergic signaling. *Trends in Neurosciences* **28**, 371-378 (2005)

5. F. Dajas-Bailador, S. Wonnacott, Nicotinic acetylcholine receptors and the regulation of neuronal signalling. *Trends in pharmacological sciences* **25**, 317-324 (2004)

6. J. J. Duan, A. F. Lozada, C. Y. Gou, J. Xu, Y. Chen, D. K. Berg, Nicotine recruits glutamate receptors to postsynaptic sites. *Molecular and cellular neurosciences* **68**, 340-349 (2015)

7. K. T. Dineley, A. A. Pandya, J. L. Yakel, Nicotinic ACh receptors as therapeutic targets in CNS disorders. *Trends in pharmacological sciences* **36**, 96-108 (2015)

8. J. M. Miwa, R. Freedman, H. A. Lester, Neural systems governed by nicotinic acetylcholine receptors: emerging hypotheses. *Neuron* **70**, 20-33 (2011)

9. H. Morishita, J. M. Miwa, N. Heintz, T. K. Hensch, Lynx1, a Cholinergic Brake, Limits Plasticity in Adult Visual Cortex. *Science* **330**, 1238-1240 (2010)

10. S. Sadigh-Eteghad, J. Mahmoudi, S. Babri, M. Talebi, Effect of alpha-7 nicotinic acetylcholine receptor activation on beta-amyloid induced recognition memory impairment. Possible role of neurovascular function. *Acta Cirurgica Brasileira* **30**, 736-742 (2015)

11. N. C. Inestrosa, J. A. Godoy, J. Y. Vargas, M. S. Arrazola, J. A. Rios, F. J. Carvajal, F. G. Serrano, G. G. Farias, Nicotine Prevents Synaptic Impairment Induced by Amyloid-β Oligomers Through α7-Nicotinic Acetylcholine Receptor Activation. *NeuroMolecular Medicine* **15**, 549-569 (2013)

12. M. Wu, J. E. Robinson, W. J. Joiner, SLEEPLESS is a bifunctional regulator of excitability and cholinergic synaptic transmission. *Current biology : CB* **24**, 621-629 (2014)

13. M. R. Picciotto, P. J. Kenny, Molecular Mechanisms Underlying Behaviors Related to Nicotine Addiction. *Cold Spring Harbor Perspectives in Medicine* **3**, (2013)

14. A. P. Govind, P. Vezina, W. N. Green, Nicotine-induced upregulation of nicotinic receptors: Underlying mechanisms and relevance to nicotine addiction. *Biochemical Pharmacology* **78**, 756-765 (2009)

15. J. Ngolab, L. Liu, R. Zhao-Shea, G. Gao, P. D. Gardner, A. R. Tapper, Functional Upregulation of alpha4* Nicotinic Acetylcholine Receptors in VTA GABAergic Neurons Increases Sensitivity to Nicotine Reward. *The Journal of neuroscience : the official journal of the Society for Neuroscience* **35**, 8570-8578 (2015)

16. S. Pons, L. Fattore, G. Cossu, S. Tolu, E. Porcu, J. M. McIntosh, J. P. Changeux, U. Maskos, W. Fratta, Crucial Role of α4 and α6 Nicotinic Acetylcholine Receptor Subunits from Ventral Tegmental Area in Systemic Nicotine Self-Administration. *The Journal of Neuroscience* **28**, 12318-12327 (2008)

17. H. A. Lester, C. Xiao, R. Srinivasan, C. D. Son, J. Miwa, R. Pantoja, M. R. Banghart, D. A. Dougherty, A. M. Goate, J. C. Wang, Nicotine is a Selective Pharmacological Chaperone of Acetylcholine Receptor Number and Stoichiometry. Implications for Drug Discovery. *The AAPS Journal* **11**, 167-177 (2009)

18. J. Sallette, S. Pons, A. Devillers-Thiery, M. Soudant, L. Prado de Carvalho, J.-P. Changeux, P. J. Corringer, Nicotine Upregulates Its Own Receptors through Enhanced Intracellular Maturation. *Neuron* **46**, 595-607 (2005)

19. B. J. Henderson, R. Srinivasan, W. A. Nichols, C. N. Dilworth, D. F. Gutierrez, E. D. Mackey, S. McKinney, R. M. Drenan, C. I. Richards, H. A. Lester, Nicotine

exploits a COPI-mediated process for chaperone-mediated up-regulation of its receptors. *The Journal of general physiology* **143**, 51-66 (2014)

20. D. H. Brunzell, J. M. McIntosh, Alpha7 Nicotinic Acetylcholine Receptors Modulate Motivation to Self-Administer Nicotine: Implications for Smoking and Schizophrenia. *Neuropsychopharmacology* **37**, 1134-1143 (2012)

21. J. L. Harenza, P. P. Muldoon, M. De Biasi, M. I. Damaj, M. F. Miles, Genetic variation within the Chrna7 gene modulates nicotine reward-like phenotypes in mice. *Genes, Brain and Behavior* **13**, 213-225 (2014)

22. V. Kumari, P. Postma, Nicotine use in schizophrenia: The self medication hypotheses. *Neuroscience & Biobehavioral Reviews* **29**, 1021-1034 (2005)

23. Z. Z. Guan, X. Zhang, K. Blennow, A. Nordberg, Decreased protein level of nicotinic receptor alpha7 subunit in the frontal cortex from schizophrenic brain. *Neuroreport* **10**, 1779-1782 (1999)

24. K. T. Dineley, M. Westerman, D. Bui, K. Bell, K. H. Ashe, J. D. Sweatt, Beta-amyloid activates the mitogen-activated protein kinase cascade via hippocampal alpha7 nicotinic acetylcholine receptors: In vitro and in vivo mechanisms related to Alzheimer's disease. *The Journal of neuroscience : the official journal of the Society for Neuroscience* **21**, 4125-4133 (2001)

25. K. Arora, J. Cheng, R. A. Nichols, Nicotinic Acetylcholine Receptors Sensitize a MAPK-linked Toxicity Pathway on Prolonged Exposure to β-Amyloid. *Journal of Biological Chemistry* **290**, 21409-21420 (2015)

26. M. S. Thomsen, M. Arvaniti, M. M. Jensen, M. A. Shulepko, D. A. Dolgikh, L. H. Pinborg, W. Hartig, E. N. Lyukmanova, J. D. Mikkelsen, Lynx1 and Abeta1-42 bind competitively to multiple nicotinic acetylcholine receptor subtypes. *Neurobiology of aging* **46**, 13-21 (2016)

27. Q. Liu, H. Kawai, D. K. Berg, beta -Amyloid peptide blocks the response of alpha 7-containing nicotinic receptors on hippocampal neurons. *Proceedings of the National Academy of Sciences of the United States of America* **98**, 4734-4739 (2001)

28. M. Mousavi, E. Hellstrom-Lindahl, Z. Z. Guan, K. R. Shan, R. Ravid, A. Nordberg, Protein and mRNA levels of nicotinic receptors in brain of tobacco using controls and patients with Alzheimer's disease. *Neuroscience* **122**, 515-520 (2003)

29. S. Oddo, A. Caccamo, K. N. Green, K. Liang, L. Tran, Y. Chen, F. M. Leslie, F. M. LaFerla, Chronic nicotine administration exacerbates tau pathology in a transgenic model of Alzheimer's disease. *Proceedings of the National Academy of Sciences of the United States of America* **102**, 3046-3051 (2005)

30. Q. Liu, X. Xie, S. Emadi, M. R. Sierks, J. Wu, A novel nicotinic mechanism underlies beta-amyloid-induced neurotoxicity. *Neuropharmacology* **97**, 457-463 (2015)

31. M. R. Picciotto, M. Zoli, Neuroprotection via nAChRs: the role of nAChRs in neurodegenerative disorders such as Alzheimer's and Parkinson's disease. *Frontiers in bioscience : a journal and virtual library* **13**, 492-504 (2008)

32. Q. Liu, B. Zhao, Nicotine attenuates β-amyloid peptide-induced neurotoxicity, free radical and calcium accumulation in hippocampal neuronal cultures. *British Journal of Pharmacology* **141**, 746-754 (2004)

33. S. Halevi, J. McKay, M. Palfreyman, L. Yassin, M. Eshel, E. Jorgensen, M. Treinin, The C. elegans ric-3 gene is required for maturation of nicotinic acetylcholine receptors. *The EMBO journal* **21**, 1012-1020 (2002)

34. S. Halevi, L. Yassin, M. Eshel, F. Sala, S. Sala, M. Criado, M. Treinin, Conservation within the RIC-3 Gene Family: EFFECTORS OF MAMMALIAN NICOTINIC ACETYLCHOLINE RECEPTOR EXPRESSION. *Journal of Biological Chemistry* **278**, 34411-34417 (2003)

35. C. A. Puddifoot, M. Wu, R. J. Sung, W. J. Joiner, Ly6h regulates trafficking of alpha7 nicotinic acetylcholine receptors and nicotine-induced potentiation of glutamatergic signaling. *The Journal of neuroscience : the official journal of the Society for Neuroscience* **35**, 3420-3430 (2015)

36. M. Wu, C. A. Puddifoot, P. Taylor, W. J. Joiner, Mechanisms of inhibition and potentiation of alpha4beta2 nicotinic acetylcholine receptors by members of the Ly6 protein family. *The Journal of biological chemistry* **290**, 24509-24518 (2015)

37. J. M. Miwa, T. R. Stevens, S. L. King, B. J. Caldarone, I. Ibanez-Tallon, C. Xiao, R. M. Fitzsimonds, C. Pavlides, H. A. Lester, M. R. Picciotto, N. Heintz, The prototoxin lynx1 acts on nicotinic acetylcholine receptors to balance neuronal activity and survival in vivo. *Neuron* **51**, 587-600 (2006)

38. I. Ibanez-Tallon, J. M. Miwa, H. L. Wang, N. C. Adams, G. W. Crabtree, S. M. Sine, N. Heintz, Novel modulation of neuronal nicotinic acetylcholine receptors by association with the endogenous prototoxin lynx1. *Neuron* **33**, 893-903 (2002)

39. W. A. Nichols, B. J. Henderson, C. Yu, R. L. Parker, C. I. Richards, H. A. Lester, J. M. Miwa, Lynx1 shifts alpha4beta2 nicotinic receptor subunit stoichiometry by affecting assembly in the endoplasmic reticulum. *The Journal of biological chemistry* **289**, 31423-31432 (2014)

40. S. Gu, J. A. Matta, B. Lord, A. W. Harrington, S. W. Sutton, W. B. Davini, D. S. Bredt, Brain alpha7 Nicotinic Acetylcholine Receptor Assembly Requires NACHO. *Neuron* **89**, 948-955 (2016)

41. J. A. Matta, S. Gu, W. B. Davini, B. Lord, E. R. Siuda, A. W. Harrington, D. S. Bredt, NACHO Mediates Nicotinic Acetylcholine Receptor Function throughout the Brain. *Cell reports* **19**, 688-696 (2017)

42. E. B. Rex, N. Shukla, S. Gu, D. Bredt, D. DiSepio, A Genome-Wide Arrayed cDNA Screen to Identify Functional Modulators of alpha7 Nicotinic Acetylcholine Receptors. *SLAS discovery* **22**, 155-165 (2017)

43. F. Wichern, M. M. Jensen, D. Z. Christensen, J. D. Mikkelsen, M. C. Gondre-Lewis, M. S. Thomsen, Perinatal nicotine treatment induces transient increases in NACHO protein levels in the rat frontal cortex. *Neuroscience* **346**, 278-283 (2017)

44. V. I. Tsetlin, Three-finger snake neurotoxins and Ly6 proteins targeting nicotinic acetylcholine receptors: pharmacological tools and endogenous modulators. *Trends in pharmacological sciences* **36**, 109-123 (2015)

45. Y. Tirosh, D. Ofer, T. Eliyahu, M. Linial, Short toxin-like proteins attack the defense line of innate immunity. *Toxins* **5**, 1314-1331 (2013)

46. J. Arredondo, A. I. Chernyavsky, D. L. Jolkovsky, R. J. Webber, S. A. Grando, SLURP-2: A novel cholinergic signaling peptide in human mucocutaneous epithelium. *Journal of cellular physiology* **208**, 238-245 (2006)

47. F. Chimienti, R. C. Hogg, L. Plantard, C. Lehmann, N. Brakch, J. Fischer, M. Huber, D. Bertrand, D. Hohl, Identification of SLURP-1 as an epidermal neuromodulator explains the clinical phenotype of Mal de Meleda. *Hum Mol Genet* **12**, 3017-3024 (2003)

48. J. G. Yamauchi, A. Nemecz, Q. T. Nguyen, A. Muller, L. F. Schroeder, T. T. Talley, J. Lindstrom, D. Kleinfeld, P. Taylor, Characterizing ligand-gated ion channel receptors with genetically encoded Ca2++ sensors. *PloS one* **6**, e16519 (2011)

49. E. N. Lyukmanova, Z. O. Shenkarev, M. A. Shulepko, K. S. Mineev, D. D'Hoedt, I. E. Kasheverov, S. Y. Filkin, A. P. Krivolapova, H. Janickova, V. Dolezal, D. A. Dolgikh, A. S. Arseniev, D. Bertrand, V. I. Tsetlin, M. P. Kirpichnikov, NMR Structure and Action on Nicotinic Acetylcholine Receptors of Water-soluble Domain of Human LYNX1. *Journal of Biological Chemistry* **286**, 10618-10627 (2011)

50. M. Wu, C. Z. Liu, W. J. Joiner, Structural Analysis and Deletion Mutagenesis Define Regions of QUIVER/SLEEPLESS that Are Responsible for Interactions with Shaker-Type Potassium Channels and Nicotinic Acetylcholine Receptors. *PloS one* **11**, e0148215 (2016)

51. R. Schoepfer, W. G. Conroy, P. Whiting, M. Gore, J. Lindstrom, Brain α-bungarotoxin binding protein cDNAs and MAbs reveal subtypes of this branch of the ligand-gated ion channel gene superfamily. *Neuron* **5**, 35-48 (1990)

52. S. Couturier, D. Bertrand, J.-M. Matter, M.-C. Hernandez, S. Bertrand, N. Millar, S. Valera, T. Barkas, M. Ballivet, A neuronal nicotinic acetylcholine receptor subunit (α7) is developmentally regulated and forms a homo-oligomeric channel blocked by α-BTX. *Neuron* **5**, 847-856 (1990)

53. D. Chen, J. W. Patrick, The alpha-bungarotoxin-binding nicotinic acetylcholine receptor from rat brain contains only the alpha7 subunit. *The Journal of biological chemistry* **272**, 24024-24029 (1997)

54. E. D. Levin, F. J. McClernon, A. H. Rezvani, Nicotinic effects on cognitive function: behavioral characterization, pharmacological specification, and anatomic localization. *Psychopharmacology* **184**, 523-539 (2006)

55. L. F. Martin, W. R. Kem, R. Freedman, Alpha-7 nicotinic receptor agonists: potential new candidates for the treatment of schizophrenia. *Psychopharmacology* **174**, 54-64 (2004)

56. F. A. Dajas-Bailador, P. A. Lima, S. Wonnacott, The alpha7 nicotinic acetylcholine receptor subtype mediates nicotine protection against NMDA excitotoxicity in primary hippocampal cultures through a Ca(2+) dependent mechanism. *Neuropharmacology* **39**, 2799-2807 (2000)

57. J. Corradi, C. Bouzat, Understanding the Bases of Function and Modulation of alpha7 Nicotinic Receptors: Implications for Drug Discovery. *Molecular pharmacology* **90**, 288-299 (2016)

58. T. L. Wallace, R. H. P. Porter, Targeting the nicotinic alpha7 acetylcholine receptor to enhance cognition in disease. *Biochemical Pharmacology* **82**, 891-903 (2011)

59. J. R. A. Wooltorton, V. I. Pidoplichko, R. S. Broide, J. A. Dani, Differential Desensitization and Distribution of Nicotinic Acetylcholine Receptor Subtypes in Midbrain Dopamine Areas. *The Journal of Neuroscience* **23**, 3176 (2003)

60. M. W. Quick, R. A. Lester, Desensitization of neuronal nicotinic receptors. *Journal of neurobiology* **53**, 457-478 (2002)

61. T. Dean, R. Xu, W. Joiner, A. Sehgal, T. Hoshi, Drosophila QVR/SSS Modulates the Activation and C-Type Inactivation Kinetics of Shaker K+ Channels. *The Journal of neuroscience : the official journal of the Society for Neuroscience* **31**, 11387-11395 (2011)

62. M. N. Wu, W. J. Joiner, T. Dean, Z. Yue, C. J. Smith, D. Chen, T. Hoshi, A. Sehgal, K. Koh, SLEEPLESS, a Ly-6/neurotoxin family member, regulates the levels, localization and activity of Shaker. *Nat Neurosci* **13**, 69-75 (2010)

63. T. J. Fleming, C. O'hUigin, T. R. Malek, Characterization of two novel Ly-6 genes. Protein sequence and potential structural similarity to alpha-bungarotoxin and other neurotoxins. *J Immunol* **150**, 5379-5390 (1993)

64. A. Galat, The three-fingered protein domain of the human genome. *Cell. Mol. Life Sci.* **65**, 3481-3493 (2008)

65. J. W. Wang, J. M. Humphreys, J. P. Phillips, A. J. Hilliker, C. F. Wu, A novel leg-shaking Drosophila mutant defective in a voltage-gated K(+)current and hypersensitive to reactive oxygen species. *The Journal of neuroscience : the official journal of the Society for Neuroscience* **20**, 5958-5964 (2000)

66. K. Koh, W. J. Joiner, M. N. Wu, Z. Yue, C. J. Smith, A. Sehgal, Identification of SLEEPLESS, a sleep-promoting factor. *Science* **321**, 372-376 (2008)

67. C. Cirelli, D. Bushey, S. Hill, R. Huber, R. Kreber, B. Ganetzky, G. Tononi, Reduced sleep in Drosophila Shaker mutants. *Nature* **434**, 1087-1092 (2005)

68. J. W. Wang, C. F. Wu, Modulation of the frequency response of Shaker potassium channels by the quiver peptide suggesting a novel extracellular interaction mechanism. *Journal of neurogenetics* **24**, 67-74 (2010)

69. R. S. Holmes, L. A. Cox, Comparative studies of glycosylphosphatidylinositol-anchored high-density lipoprotein-binding protein 1: evidence for a eutherian mammalian origin for the GPIHBP1 gene from an LY6-like gene. *3 Biotech* **2**, 37-52 (2012)

70. R. Loertscher, P. Lavery, The role of glycosyl phosphatidyl inositol (GPI)-anchored cell surface proteins in T-cell activation. *Transpl Immunol* **9**, 93-96 (2002)

71. W. Plengpanich, S. G. Young, W. Khovidhunkit, A. Bensadoun, H. Karnman, M. Ploug, H. Gardsvoll, C. S. Leung, O. Adeyo, M. Larsson, S. Muanpetch, S. Charoen, L. G. Fong, S. Niramitmahapanya, A. P. Beigneux, Multimerization of GPIHBP1 and Familial Chylomicronemia from a Serine-to-Cysteine Substitution in GPIHBP1's Ly6 Domain. *Journal of Biological Chemistry*, (2014)

72. A. P. Govind, H. Walsh, W. N. Green, Nicotine-Induced Upregulation of Native Neuronal Nicotinic Receptors Is Caused by Multiple Mechanisms. *The Journal of Neuroscience* **32**, 2227 (2012)

73. A. Kuryatov, J. Luo, J. Cooper, J. Lindstrom, Nicotine acts as a pharmacological chaperone to up-regulate human alpha4beta2 acetylcholine receptors. *Molecular pharmacology* **68**, 1839-1851 (2005)

74. O. Adeyo, M. Oberer, M. Ploug, L. G. Fong, S. G. Young, A. P. Beigneux, Heterogeneity in the Properties of Mutant SLURP1 Proteins in Mal de Meleda. *Br J Dermatol*, (2015)

75. M. Mallya, R. D. Campbell, B. Aguado, Characterization of the five novel Ly-6 superfamily members encoded in the MHC, and detection of cells expressing their potential ligands. *Protein Sci.* **15**, 2244-2256 (2006)

76. A. B. Tekinay, Y. Nong, J. M. Miwa, I. Lieberam, I. Ibanez-Tallon, P. Greengard, N. Heintz, A role for LYNX2 in anxiety-related behavior. *Proc Natl Acad Sci USA* **106**, 4477-4482 (2009)

77. K. B. Abbitt, M. J. Cotter, V. C. Ridger, D. C. Crossman, P. G. Hellewell, K. E. Norman, Antibody ligation of murine Ly-6G induces neutropenia, blood flow cessation, and death via complement-dependent and independent mechanisms. *J Leukoc Biol* **85**, 55-63 (2009)

78. S. B. Bradfute, T. A. Graubert, M. A. Goodell, Roles of Sca-1 in hematopoietic stem/progenitor cell function. *Exp Hematol* **33**, 836-843 (2005)

79. C. Bresson-Mazet, O. Gandrillon, S. Gonin-Giraud, Stem cell antigen 2: a new gene involved in the self-renewal of erythroid progenitors. *Cell Prolif* **41**, 726-738 (2008)

80. N. Kiguchi, Y. Kobayashi, T. Maeda, S. Tominaga, J. Nakamura, Y. Fukazawa, M. Ozaki, S. Kishioka, Activation of nicotinic acetylcholine receptors on bone marrow-derived cells relieves neuropathic pain accompanied by peripheral neuroinflammation. *Neurochemistry International* **61**, 1212-1219 (2012)

81. P. Y. Lee, J.-X. Wang, E. Parisini, C. C. Dascher, P. A. Nigrovic, Ly6 family proteins in neutrophil biology. *J Leukoc Biol* **94**, 585-594 (2013)

82. K. K. Long, M. Montano, G. K. Pavlath, Sca-1 is negatively regulated by TGF-beta1 in myogenic cells. *FASEB J* **25**, 1156-1165 (2011)

83. Y. Bourne, T. T. Talley, S. B. Hansen, P. Taylor, P. Marchot, Crystal structure of a Cbtx-AChBP complex reveals essential interactions between snake alpha-neurotoxins and nicotinic receptors. *EMBO J* **24**, 1512-1522 (2005)

84. C. D. Dellisanti, Y. Yao, J. C. Stroud, Z.-Z. Wang, L. Chen, Crystal structure of the extracellular domain of nAChR alpha1 bound to alpha-bungarotoxin at 1.94 A resolution. *Nature Neuroscience* **10**, 953-962 (2007)

85. E. N. Lyukmanova, M. A. Shulepko, S. L. Buldakova, I. E. Kasheverov, Z. O. Shenkarev, R. V. Reshetnikov, S. Y. Filkin, D. S. Kudryavtsev, L. O. Ojomoko, E. V. Kryukova, D. A. Dolgikh, M. P. Kirpichnikov, P. D. Bregestovski, V. I. Tsetlin, Water-soluble LYNX1 Residues Important for Interaction with Muscle-type and/or Neuronal Nicotinic Receptors. *Journal of Biological Chemistry* **288**, 15888-15899 (2013)

86. N. Unwin, Refined structure of the nicotinic acetylcholine receptor at 4A resolution. *J Mol Biol* **346**, 967-989 (2005)

87. S. B. Long, E. B. Campbell, R. Mackinnon, Crystal structure of a mammalian voltage-dependent Shaker family K+ channel. *Science* **309**, 897-903 (2005)

88. F. A. Dajas-Bailador, L. Soliakov, S. Wonnacott, Nicotine activates the extracellular signal-regulated kinase 1/2 via the alpha7 nicotinic acetylcholine receptor and protein kinase A, in SH-SY5Y cells and hippocampal neurones. *J Neurochem* **80**, 520-530 (2002)

89. R. Srinivasan, R. Pantoja, F. J. Moss, E. D. Mackey, C. D. Son, J. Miwa, H. A. Lester, Nicotine up-regulates α4β2 nicotinic receptors and ER exit sites via stoichiometry-dependent chaperoning. *The Journal of general physiology* **137**, 59-79 (2011)

90. T. A. Murray, Q. Liu, P. Whiteaker, J. Wu, R. J. Lukas, Nicotinic acetylcholine receptor [alpha]7 subunits with a C2 cytoplasmic loop yellow fluorescent protein insertion form functional receptors. *Acta Pharmacol Sin* **30**, 828-841 (2009)

91. R. F. Margolskee, B. McHendry-Rinde, R. Horn, Panning transfected cells for electrophysiological studies. *BioTechniques* **15**, 906-911 (1993)